Key Points:

- We present two well-replicated tree-ring oxygen isotope ($\delta^{18}O_{TR}$) records from tropical South America spanning the past two centuries
- These records capture important large-scale climate signals, including interannual variation in Amazon basin-wide precipitation
- A multi-decadal long-term increase in $\delta^{18}O_{TR}$ is interpreted as being primarily driven by a long-term reduction in rainout fraction

Supporting Information:

Supporting Information may be found in the online version of this article.

Correspondence to:

J. C. A. Baker,
j.c.baker@leeds.ac.uk

The Changing Amazon Hydrological Cycle—Inferences From Over 200 Years of Tree-Ring Oxygen Isotope Data

Jessica C. A. Baker[1] , Bruno B. L. Cintra[2] , Manuel Gloor[3] , Arnoud Boom[4] , David Neill[5] , Santiago Clerici[1], Melanie J. Leng[6] , Gerhard Helle[7], and Roel J. W. Brienen[3]

[1]School of Earth and Environment, University of Leeds, Leeds, UK, [2]School of Geography, Earth and Environmental Sciences, Birmingham Institute of Forest Research (BIFoR), University of Birmingham, UK, [3]School of Geography, University of Leeds, Leeds, UK, [4]School of Geography, Geology and the Environment, University of Leicester, Leicester, UK, [5]Universidad Estatal Amazónica, Puyo, Ecuador, [6]National Environmental Isotope Facility, British Geological Survey, Keyworth, UK, [7]Section 4.3 Climate Dynamics and Landscape Evolution, GFZ—German Research Centre for Geosciences, Telegrafenberg, Germany

Abstract Changes to the Amazon hydrological cycle have important consequences for world's largest tropical forest, and the biodiversity it contains. However, a scarcity of long-term climate data in the region makes it hard to contextualize recent observed changes in Amazon hydrology. Here, we explore to what extent tree-ring oxygen isotope ($\delta^{18}O_{TR}$) chronologies can inform us about hydrological changes in the Amazon over the past two centuries. Two $\delta^{18}O_{TR}$ records from northern Bolivia and the Ecuadorian Andes are presented. The Ecuador record spans 1799–2012 ($n = 16$ trees) and the Bolivia record spans 1860–2014 ($n = 32$ trees), making them the longest $\delta^{18}O_{TR}$ records from the Amazon, and among the most highly-replicated $\delta^{18}O_{TR}$ records from the tropics to date. The two chronologies correlate well at interannual and decadal timescales, despite coming from sites more than 1,500 km apart. Both $\delta^{18}O_{TR}$ records are strongly related to interannual variation in Amazon River discharge measured at Óbidos, and accumulated upwind precipitation, suggesting a common climatic driver. In both records a strong increase in $\delta^{18}O_{TR}$ was observed up until approximately 1950, consistent with positive trends in the few other existing $\delta^{18}O$ proxy records from across the Amazon. Considering all possible drivers of this long-term increase, a reduction in rainout fraction over the basin driven by rising sea surface temperatures in the North Atlantic is suggested as the most likely cause. The upward trend in $\delta^{18}O_{TR}$ reverses over the past 1–2 decades, consistent with the observed strengthening of the Amazon hydrological cycle since approximately 1990.

Plain Language Summary Long-term climate measurements from the Amazon are few and far between, so information about the climate in the past needs to come from alternative sources. This is essential to provide context for current climate variability such as the strengthening of the Amazon water cycle since the 1990s. One way we can reconstruct historical climate is using stable oxygen isotopes recorded in tree rings. Previous work has shown that tree-ring oxygen isotopes from the western Amazon can tell you about the amount of rainfall over the entire basin. Here, we present tree-ring isotope records from Ecuador and Bolivia that span the past two centuries, making them the longest tree-ring oxygen isotope records from the region to date. We find that the two records are very similar to one another, despite coming from sites that are more than 1,500 km apart, suggesting they are both influenced by the same climatic factors. We explore the climate signals that these records contain, including interpreting a long-term positive trend in the isotope record until around 1950. We conclude that the most likely cause of this trend is a long-term reduction in the fraction of incoming water vapor that falls as rainfall over the Amazon.

1. Introduction

The water and carbon cycles are closely coupled in the Amazon basin, which is the largest freshwater drainage basin in the world. Perturbations in one cycle can therefore have important consequences for the other (Gatti et al., 2014; Lewis et al., 2011; Marengo & Espinoza, 2016; Phillips et al., 2009). The fate of Amazon vegetation under future change scenarios has been the subject of much discussion in the literature, with some model-based analyses suggesting climate feedbacks could cause precipitation reductions, system destabilization and possible widespread forest loss (Cox et al., 2004; Huntingford et al., 2008; Malhi et al., 2009; Zemp et al., 2017). However, analysis of rain gauge and river flux data from the region instead shows that precipitation in the Amazon during the wet season has actually increased since approximately 1990 (Gloor et al., 2013), though wet and dry season

precipitation anomalies are becoming increasingly variable (Espinoza et al., 2014; Fu et al., 2013; Marengo & Espinoza, 2016), and are projected to continue to do so into the future (Baker et al., 2021; Boisier et al., 2015).

Despite the importance of assessing climate change for the conservation of carbon stocks and biodiversity, the number of monitoring stations in the Amazon reporting weather data has fallen since the late 1980s (exemplified by the number of Amazon stations incorporated in the Climatic Research Unit precipitation record, Harris et al., 2014), and there are few century-scale instrumental records. This makes it hard to assess recent changes in hydrology in the context of historic variability. Proxy climate data, such as oxygen isotope ratios ($\delta^{18}O$), can potentially provide some insight on past hydrological variation (Vuille et al., 2012). For example, there have been a growing number of speleothem $\delta^{18}O$ records from the Amazon in recent years (Kanner et al., 2013; Moquet et al., 2016; Novello et al., 2016; Wang et al., 2017; Ward et al., 2019; Wong et al., 2021), though these often have low replication and highly variable temporal resolution (e.g., <1–150 years). Therefore, there is a need to identify other tropical proxies that can provide a reliable record of on-going change, as well as helping to improve our understanding of past hydrological cycle variation.

It was shown in a previous study that $\delta^{18}O$ preserved in tree rings ($\delta^{18}O_{TR}$) from northern Bolivia correlate well with interannual variation in precipitation over the whole Amazon basin and could therefore be used to better understand Amazon hydrology in the past (Brienen et al., 2012). Trajectory modeling has been used to explain this relationship, with $\delta^{18}O_{TR}$ inversely related to the fraction of incoming water vapor that falls as precipitation over the basin (Baker et al., 2016; Cintra et al., 2021). The rainout fraction influences isotopes in precipitation ($\delta^{18}O_P$) in the Amazon: during transport of atmospheric moisture across the basin, water molecules containing heavy isotopes are more likely to condense and fall as rain, depleting the isotopic composition of water vapor remaining in the atmosphere following a Rayleigh distillation (Dansgaard, 1964; Salati et al., 1979). The $\delta^{18}O_P$ signal recorded in tree-ring cellulose therefore provides a reliable record of basin-scale precipitation variability. However, although $\delta^{18}O_{TR}$ show promise as a proxy for reconstructing interannual variation in precipitation, there have been few well-replicated $\delta^{18}O_{TR}$ chronologies from the region that extend much beyond the limit of instrumental data (Table S1 in Supporting Information S1).

While the climate controls on interannual variation in $\delta^{18}O_{TR}$ from the Amazon are relatively well understood (i.e., variation in the fraction of incoming vapor that rains out over the basin), the factors influencing long-term (i.e., multidecadal to centennial) trends have not yet been examined. Reconstructing climate from proxy data assumes that all alternative drivers of variation have remained constant through time (i.e., the assumption of uniformitarianism; Bradley, 2011). For Amazon tree rings, several factors might cause long-term changes in the recorded $\delta^{18}O$ signal besides a change in the rainout fraction. These include, biases related to tree age or size (i.e., ontogenetic effects, Mccarroll & Loader, 2004; van der Sleen et al., 2017), changes in atmospheric CO_2 or leaf-to-air vapor pressure deficit influencing plant stomatal conductance (Barbour et al., 2000; Farquhar & Lloyd, 1993), changes in seawater $\delta^{18}O$ or sea surface temperature (SST) changes influencing isotopic fractionation during evaporation from the ocean (Craig & Gordon, 1965), and climate change causing changes to the lapse rate, local amount effects or biosynthetic fractionation rate (Dansgaard, 1964; Mook, 2000; Sternberg, 2009). These potential influences on $\delta^{18}O_{TR}$ operate on different timescales to factors controlling interannual variability and need to be considered when interpreting $\delta^{18}O_{TR}$ chronologies.

In this study, we use $\delta^{18}O_{TR}$ records from the Amazon to improve our understanding of temporal variation in regional hydrology and its controls. Two annually-resolved and well-replicated $\delta^{18}O_{TR}$ chronologies from the western margin of the Amazon basin are presented. These records span the last two centuries making them the longest $\delta^{18}O_{TR}$ records from the region to date. Comparisons with climate data are made to assess whether the records are influenced by a common climatic driver. In addition to controls on interannual variability, we consider a range of factors that might influence $\delta^{18}O_{TR}$ over longer timescales and quantify the likely magnitude of each. This hypothesis-driven approach was used to investigate the cause of a long-term increase in $\delta^{18}O_{TR}$ since the early 1800s.

2. Methods

2.1. Sample Collection

This study combines samples from three lowland rainforest sites in northern Bolivia and a montane forest in the eastern Ecuadorian Andes (Figure 1). *Cedrela odorata* trees were sampled in Bolivia and the closely related
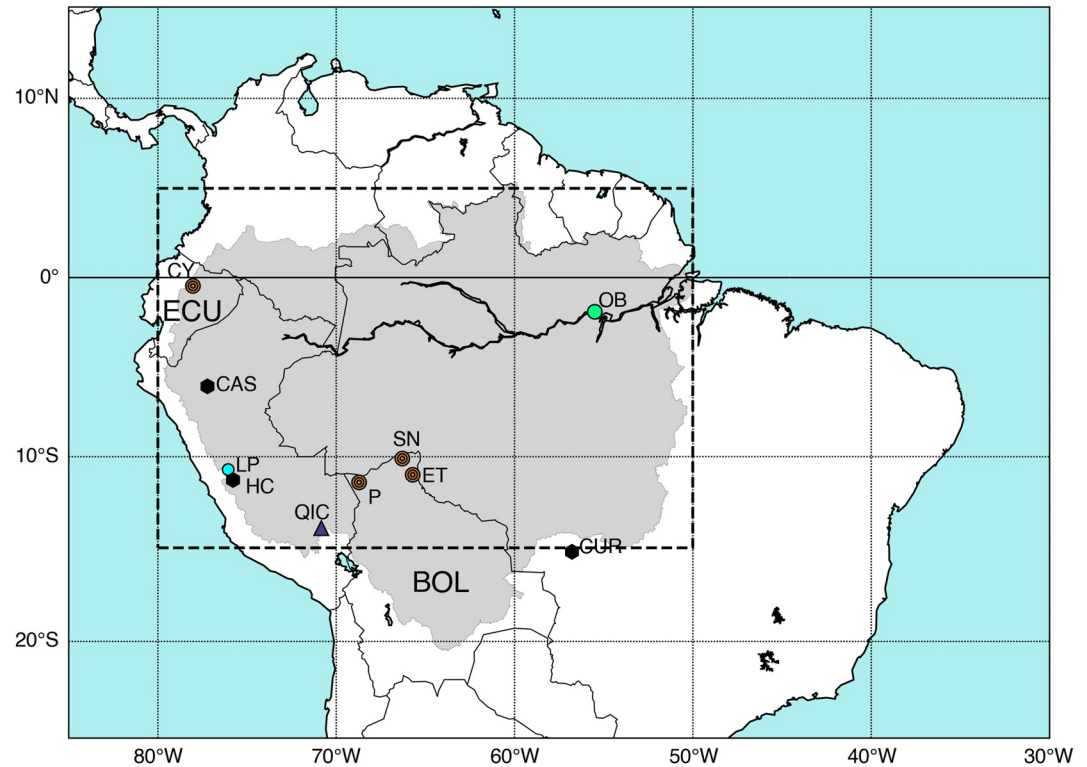
Figure 1. Map of δ^{18}O proxy records from the Amazon. The Amazon basin (gray shading), tree-ring sampling sites (brown circles; CY = Cuyuja, P = Purisima, SN = Selva Negra, ET = El Tigre), the meteorological station at Óbidos (green circle; OB) and the locations of other δ^{18}O proxy records, including records from speleothems (black hexagons; CAS = Cascayunga cave, Reuter et al., 2009; HC = Huagapo cave, Kanner et al., 2013; CUR = Curupira cave, Novello et al., 2016), a lake sediment record (blue circle; LP = Laguna Pumacocha, Bird et al., 2011) and an ice-core record (dark blue triangle; QIC = Quelccaya ice core, Thompson et al., 2013) are shown. Bolivia and Ecuador are labeled. The dashed black box indicates the area where meteorological stations contributing to CRU were counted (Figure S6 in Supporting Information S1).

species *Cedrela montana* was sampled in Ecuador. The Bolivian samples are from primary forests in Purisima (11.40°S, 68.72°W, 170 m above sea level [a.s.l.]) and Selva Negra (10.10°S, 66.31°W, 160 m a.s.l.), and a secondary forest in El Tigre (10.98°S, 65.72°W, 165 m above mean sea level [AMSL]). The δ^{18}O$_{TR}$ chronologies from Purisima and Selva Negra have been presented in previous publications (Baker et al., 2015, 2016; Brienen et al., 2012), though the present study uses additional samples and extends the analysis further back in time. All of the Bolivia sites are located relatively close together and thus have a similar climate. Total annual precipitation is approximately 1,700 mm and highly seasonal, with a wet season (defined here as months with precipitation >100 mm) from October to April, which coincides with the main growing season for trees here (Brienen & Zuidema, 2005). Mean annual temperature is 26.2°C with little seasonal variation (climate data are from 1960 to 2004, from the Riberalta meteorological station in the Global Historical Climatology Network-Monthly [GHCN-M] database Peterson & Vose, 1997 accessed via KNMI [Koninklijk Nederlands Meteorologisch Instituut] Climate Explorer: http://climexp.knmi.nl).

The Ecuadorian samples are from Cuyuja (0.45°S, 78.04°W), which is at high elevation (2,950 m AMSL) with more variable topography. This site is much cooler than the Bolivian lowland sites (mean annual temperature is 10.5°C). The Cuyuja δ^{18}O$_{TR}$ record was presented in a short comment piece (Baker et al., 2018) but has not previously been analyzed in detail. Annual precipitation at Cuyuja is approximately 1,500 mm, which is similar to that of the Bolivian sites, though precipitation seasonality is lower in Ecuador (climate data are from the Papallacta meteorological station (3,150 m a.s.l., 20 km away from sample site) from the period 1949–2008 (discontinuous) and available from the INAMHI (Instituto Nacional de Meteorologia e Hidrologia): http://www.serviciometeoro-logico.gob.ec). The wet season in Cuyuja is from March to September, and although there are no observations of leaf phenology or seasonal growth rhythms in this location, studies have shown that *C. montana* trees in southern

Ecuador grow from December/January to April/May (Bräuning et al., 2009) before losing their leaves, with senescence possibly triggered by reduced light intensities at the height of the wet season (Bräuning et al., 2008).

Stem discs were collected from Purisima in 2002, from Selva Negra in 2011 and from Cuyuja in 2013, from trees that had been felled in the same year. Living trees in Selva Negra and Cuyuja were also sampled using a 10-mm increment borer to collect cores approximately 130 cm from the ground in 2–4 directions around the circumference of the tree. In 2015 cores were also taken from living trees in El Tigre to capture more recent tree growth.

2.2. Sample Preparation

Discs were polished with sandpaper (up to grit 600) using a Bosch orbital sander, to improve the visibility of the tree rings. On each disc, rings were counted along 2–4 radii, with every 10th ring interconnected between radii to ensure that no rings had been missed or misidentified. This was particularly important in samples from Ecuador where wedging (locally absent) rings were common. Furthermore, rings were very compressed in the outside edge of some discs, due to slow growth of large trees. The oldest discs with the clearest rings were selected for isotope analysis (17 discs from Bolivia and 10 discs from Ecuador). Cores from younger trees were also analyzed to assess the effect of ontogeny on $\delta^{18}O_{TR}$ signals. Cores were prepared using a core-microtome (Gärtner & Nievergelt, 2010) and on each core rings were marked and measured in the perpendicular direction to the ring boundaries using a LINTAB measuring stage. Ring widths were visually cross-dated (Stokes & Smiley, 1968) between 2 and 4 cores from each tree to identify where rings might have been missed/misidentified. Cores with the widest and clearest rings were chosen for isotope analysis (17 cores from Bolivia and 13 cores from Ecuador).

Isotope analysis was conducted on α-cellulose, which was extracted from whole wood using two different methods. Samples from Bolivia were prepared using a scalpel to isolate and cut up the wood from each individual tree ring, making sure that the full width of the ring was evenly sampled. Wood from each ring was then put into separate filter funnel and cellulose extraction was conducted following the batch method of Wieloch et al. (2011). After extraction cellulose samples were transferred to Eppendorf tubes for homogenization using a Retsch MM 301 mixer mill and then freeze-dried before being packed into silver cups for isotope analysis (see Section 2.3).

The samples from Ecuador were analyzed following an alternative technique whereby cellulose is extracted before the rings are separated from each other. We followed a protocol based on the methods of Kagawa et al. (2015) and Li et al. (2011), which builds on earlier work by Loader et al. (2002). In brief, a bandsaw was used to cut sections of wood approximately 10 mm wide, 1 mm thick and between 50 and 100 mm long. These wood laths were scanned at high resolution and then sewn into perforated polytetrafluoroethylene (PTFE) cases, prior to chemical treatment to extract the cellulose following the procedure of Wieloch et al. (2011). This methodology permits much higher throughput of samples (on the order of 1,000 rings per week) compared to conventional approaches (on the order of 100 rings per week). After extraction, the cellulose laths were freeze-dried while still inside their PTFE cases. Dried laths were inspected using a stereomicroscope with a transparent stage and mirror to reflect transmitted light and optimize ring visibility. Rings were carefully separated using a scalpel with reference to the wood scans to identify each ring correctly. Purified cellulose from each ring was then homogenized and freeze-dried as above, before being packed into silver cups.

A comparison between the two cellulose extraction methods was conducted with a series of 21 rings from a tree from Cuyuja, Ecuador (Text S1 and Figure S1 in Supporting Information S1). $\delta^{18}O_{TR}$ values from the two methods correlate reasonably well ($R^2 = 0.76$) and the slope and intercept of the regression do not differ significantly from 1 and 0 respectively (slope = 0.83 ± 0.22, intercept = 3.33 ± 5.33, 95% confidence intervals). However, the cross-section method gave consistently lower $\delta^{18}O_{TR}$ values, (mean offset = 0.8‰, root mean square error = 0.98‰, n = 21). Due to this offset, it was decided that cellulose $\delta^{18}O$ values from the two methods would not be combined into a single $\delta^{18}O_{TR}$ chronology. Finally, slight differences in $\delta^{18}O$ values obtained from these two approaches would not affect the main conclusions drawn in this study, as these relate to drivers of inter-annual variability and long-term trends in $\delta^{18}O_{TR}$, which would not be influenced by an offset in absolute values.

2.3. Oxygen Isotope Analysis

The isotope series presented here were measured in four laboratories. Samples from Purisima were analyzed at the German Research Center for Geosciences (GFZ) in Potsdam, Germany; Selva Negra samples were analyzed

at the British Geological Survey's Stable Isotope Facility (part of the NERC National Environmental Isotope Facility, NEIF) in Keyworth, Nottingham, UK; the El Tigre samples were analyzed at the University of Leeds; and Ecuador samples were analyzed at the University of Leicester. Methods for $\delta^{18}O$ analysis at GFZ, NEIF and Leeds have been described at length in a previous study (Baker et al., 2015), thus for brevity we only describe the methods employed at the University of Leicester.

Cellulose $\delta^{18}O$ values were determined by pyrolysis in a high temperature (HT) furnace equipped with a glassy carbon reactor. Cellulose encapsulated in silver cups was converted to CO at a temperature of 1,350°C using a Sercon HT furnace coupled to a Sercon Hydra 20-20 continuous flow isotope-ratio mass spectrometer (IRMS). $\delta^{18}O$ values (where $\delta = (((^{18}O/^{16}O_{sample})/(^{18}O/^{16}O_{standard})) - 1) \times 1,000)$ were calculated with reference to cellulose from Sigma-Aldrich, UK (Lot#SLBD2972V, VSMOW = 29.8‰). Precision was typically <0.2‰ (calculated across 26 batches with 6 samples per batch).

2.4. Dating $\delta^{18}O_{TR}$ Series

Cross-dating $\delta^{18}O_{TR}$ series against an established $\delta^{18}O_{TR}$ chronology from the same region has been shown to be a cheap and effective way to verify tree-ring dates (Baker et al., 2015). $\delta^{18}O_{TR}$ chronologies from Purisima and Selva Negra have already been established (Baker et al., 2015; Brienen et al., 2012), and new $\delta^{18}O_{TR}$ records from Selva Negra and El Tigre were aligned with these published records. Where dating errors were suspected, the original samples of wood were re-inspected to see whether any tree rings had been missed or miscounted. For the development of the Ecuador $\delta^{18}O_{TR}$ chronology a different procedure was followed: trees were matched against each other, since the site at Cuyuja is too far (>1,500 km) from the Bolivia sites to assume that trees show similar interannual $\delta^{18}O_{TR}$ signals. For both sites, statistical cross-dating of $\delta^{18}O_{TR}$ series of the individual trees was conducted using TSAP-Win software and its cross-dating statistics (Gleichläufigkeit and correlations). Some errors in the initial ring counting were found during cross-dating - these were identified on the original whole disks as locally-absent tree rings (i.e., wedging rings) caused by dormant cambium in some sections of the disc (Brienen et al., 2016). Some of the $\delta^{18}O_{TR}$ data from increment cores (from Ecuador and the Bolivian El Tigre site) could not be cross-dated, probably due to the high incidence of wedging rings, which could only be identified by careful scrutiny of complete discs. The non-matching series, which were all from small trees (two from El Tigre and seven from Cuyuja), were excluded from the composite chronologies.

Finally, one tree from Selva Negra and three trees from Cuyuja were selected for "bomb-peak" radiocarbon (^{14}C) analysis to independently validate tree-ring dates. We showed in a previous study that the ^{14}C measured in tree rings from both of these sites show excellent agreement with existing ^{14}C calibration curves, proving trees have been precisely dated (Baker et al., 2017).

2.5. Data Analysis

Mean $\delta^{18}O_{TR}$ chronologies were constructed for Ecuador and Bolivia, with a minimum of three trees averaged at any point along each chronology (Figures S2 and S3; Table S2 in Supporting Information S1). The Ecuador record combines data from 16 trees (maximum replication of 12) and spans the period 1799–2012. The Bolivia record combines $\delta^{18}O_{TR}$ data from all three sites (a total of 32 trees, maximum replication of 31) and spans 1860–2014 (data from 1901 to 2010 have been published previously Baker et al., 2015, 2016; Brienen et al., 2012). $\delta^{18}O_{TR}$ signals in trees from Purisima correlate strongly with trees from Selva Negra (Baker et al., 2015). The series also have similar standard deviations (0.9 and 1.1‰ respectively), but the trees from Purisima have consistently higher $\delta^{18}O_{TR}$ (by ~2.7‰). At least 1‰ of this offset is attributable to the fact that the series were measured in different laboratories (for full details refer to the interlaboratory comparison in Baker et al., 2015). Inter-laboratory differences in absolute $\delta^{18}O_{TR}$ of up to 1‰ have also been reported previously (Boettger et al., 2007). Cellulose is water-insoluble but strongly hygroscopic, and thus the International Atomic Energy Agency (IAEA) does not provide $\delta^{18}O$ reference values for their official cellulose standards (IAEA C3 and V9) as they may change with laboratory conditions. The cause for the rest of the offset is unclear, though there are several reasons why we might expect an offset in $\delta^{18}O_{TR}$ between distant sites: it could be related to differences in soils between the two sites affecting soil water residence times, or due to physiological differences between sub-populations of *C. odorata*. These site-specific influences on $\delta^{18}O_{TR}$ would not be expected to change over time: indeed, we found no long-term trend in the offset magnitude (Figure S4 in Supporting Information S1). Before constructing the

mean chronology for Bolivia all Purisima $\delta^{18}O_{TR}$ values were offset by 2.7‰ to standardize the means between the different sites. Offsetting data by a constant value in this way would not affect the main findings presented in this study, as it does not affect the temporal variability of $\delta^{18}O_{TR}$ at interannual or multi-decadal timescales.

Mean inter-tree correlation coefficients (r_{mean}) and "Expressed Population Signal" (EPS) statistics were used to measure $\delta^{18}O_{TR}$ chronology reliability. EPS is a measure of the extent to which a chronology is dominated by individual tree-level (EPS < 0.85) or stand-level (EPS > 0.85) signals (Wigley et al., 1984) and is calculated using the formula:

$$EPS = (N * r_{mean})/(1 + (N - 1) * r_{mean})$$

where N is the number of individual trees. A moving-window analysis was used to calculate running r_{mean} and EPS statistics, using a window of 30 years, to show changes in chronology quality through time. Inclusion of the eight Purisima trees made little difference to the running mean and EPS of the Bolivia chronology (Figure S5 in Supporting Information S1).

$\delta^{18}O_{TR}$ records were compared against each other, and with climate data, to identify controls at interannual, decadal and centennial timescales. Spatial correlation analyses were performed to reveal relationships between $\delta^{18}O_{TR}$ records and regional climate. All correlations presented use the Pearson's product-moment correlation method and are between the unfiltered, interannual time series, unless otherwise indicated. Linear trends were identified using ordinary least squares (OLS) regression. To visualize low frequency trends in $\delta^{18}O_{TR}$ records and climate data, a second order, low-pass Butterworth filter with a cut-off frequency of 0.2 was applied in forward and reverse directions to each data series.

Climate data were downloaded via KNMI Climate Explorer, unless otherwise stated. Monthly precipitation and temperature observations (1901–2015) come from the Climatic Research Unit (CRU) TS3.24.01 product at 0.5° × 0.5° resolution (Harris et al., 2014). Spatial correlation analyses only used CRU data from the period 1953–1989 when the interpolated precipitation product includes data from >50 stations in the Amazon region (defined here as 15°S–5°N, 50–80°W, Figure S6 in Supporting Information S1). Monthly SST data are from the National Oceanic and Atmospheric Administration (NOAA) Extended Reconstruction Sea Surface Temperature (ERSST) data set version 4 at 2° × 2° resolution (Huang et al., 2015). ERSST data were used from 1880 onwards, due to increasing uncertainty before this time (Huang et al., 2016). In addition, reconstructed North Atlantic SST anomalies for the period 1799–2006 from Mann et al. (2009) were used. This reconstructed data set is based on multiple proxy records, including tree rings, ice cores, corals, speleothems and marine sediments. Monthly Amazon flow data, measured at Óbidos, are from the Agência Nacional de Águas (ANA) in Brazil (HidroWeb, 2018), with missing values reconstructed using linear relationships with hydrometric data from stations at Taperinha and Manaus (Antico & Torres, 2015).

3. Results and Discussion

3.1. Record Description and Inter-Comparison

The $\delta^{18}O_{TR}$ timeseries and composite chronologies from Ecuador and Bolivia are presented in Figure 2. These records span two centuries (1799–2014) and are the longest and among the best-replicated $\delta^{18}O_{TR}$ records from tropical South America to date (Table S1 in Supporting Information S1). The *C. odorata* trees comprising the Bolivia chronology show high inter-tree synchronicity in $\delta^{18}O_{TR}$ ($r_{mean} = 0.69$) and an EPS of 0.99 (Figure 2b and Figure S2 in Supporting Information S1), which strongly indicates that $\delta^{18}O_{TR}$ signals are governed by an external control. There is slightly more variability between *C. montana* $\delta^{18}O_{TR}$ series from Ecuador ($r_{mean} = 0.45$), possibly due to greater topographic variation at the montane site introducing variation in the amount of mixing between recent precipitation and residual groundwater for trees growing at different elevations. However, an EPS of 0.93 (Figure 2a) still suggests that the chronology is dominated by stand-level influences (Wigley et al., 1984). Moving window r_{mean} and EPS statistics decline for the most recent part of the Ecuador chronology (Figure S3 in Supporting Information S1), probably due to the inclusion of the six increment cores, which could not be as carefully dated as the discs (see Section 2.4), and because the rings in the discs tended to be very compressed in the outside edge, possibly resulting in errors during ring counting or when isolating the cellulose from each ring. However, in general both chronologies are well replicated, show coherent signals between trees and are sufficiently robust for further analysis.
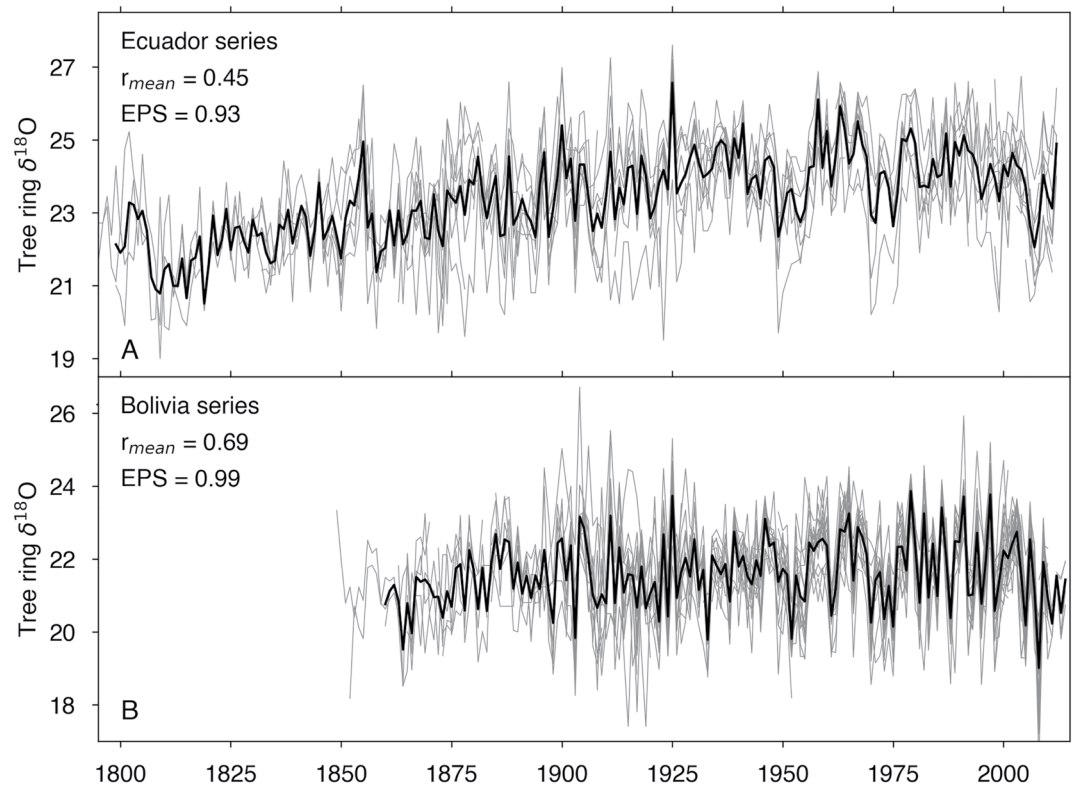
Figure 2. New $\delta^{18}O_{TR}$ chronologies from Ecuador and Bolivia. Gray lines represent individual trees (16 for Ecuador and 32 for Bolivia) and the black lines show the mean composite chronologies. The mean inter-tree correlation (r_{mean}) and expressed population signal values for the composite chronologies are indicated.

The Ecuador and Bolivia records correlate well at interannual timescales ($r = 0.57$, $p < 0.001$, 1860–2012, $n = 153$), despite coming from sites which are >1500 km apart and have an elevation difference of approximately 2750 m. Low-pass filters applied to the records also reveal close similarities in their decadal and long-term trends (Figure S4 in Supporting Information S1). Correlations between nearby $\delta^{18}O_{TR}$ records can be caused by changes in local relative humidity (RH) affecting stomatal conductance and consequently leaf water isotope enrichment (Andreu-Hayles et al., 2016; Labuhn et al., 2014; Xu et al., 2011). However, the large distance between the sample sites suggests a basin-scale climatic control on the signal, which is independent of local conditions.

3.2. What Drives Interannual and Decadal Variation in $\delta^{18}O_{TR}$ From Ecuador?

The climatic factors controlling interannual variation in $\delta^{18}O_{TR}$ records from northern Bolivia are already well understood (Baker et al., 2016; Brienen et al., 2012): the rainout of heavy isotopes during moisture transport across the Amazon basin, and strong recycling of water vapor through vegetation, drive variation in precipitation $\delta^{18}O$ ($\delta^{18}O_P$) (Dansgaard, 1964; Insel et al., 2013; Pierrehumbert, 1999; Salati et al., 1979; Villacís et al., 2008; Vimeux et al., 2005) and this signal is recorded in cellulose with minimal modification in response to local climate effects (Barbour et al., 2004). Similarity between $\delta^{18}O_{TR}$ records from distant sites, and between $\delta^{18}O_{TR}$ and other stable isotope proxy records, has been reported before in the Amazon (Baker et al., 2015; Ballantyne et al., 2011; Brienen et al., 2012; Volland et al., 2016) and has been attributed to strong regional coherence in $\delta^{18}O_P$, caused by the link between basin precipitation amount and the strength of the South America monsoon (Nobre et al., 2009). The Ecuador and Bolivia $\delta^{18}O_{TR}$ chronologies correlate well with each other and since both records are from the far west of the basin, it is likely they are controlled by a similar mechanism, though this has yet to be shown. The following section focuses on identifying the factors controlling interannual and decadal variation in Ecuador $\delta^{18}O_{TR}$ and show how these differ from or relate to the known controls on $\delta^{18}O_{TR}$ from Bolivia.
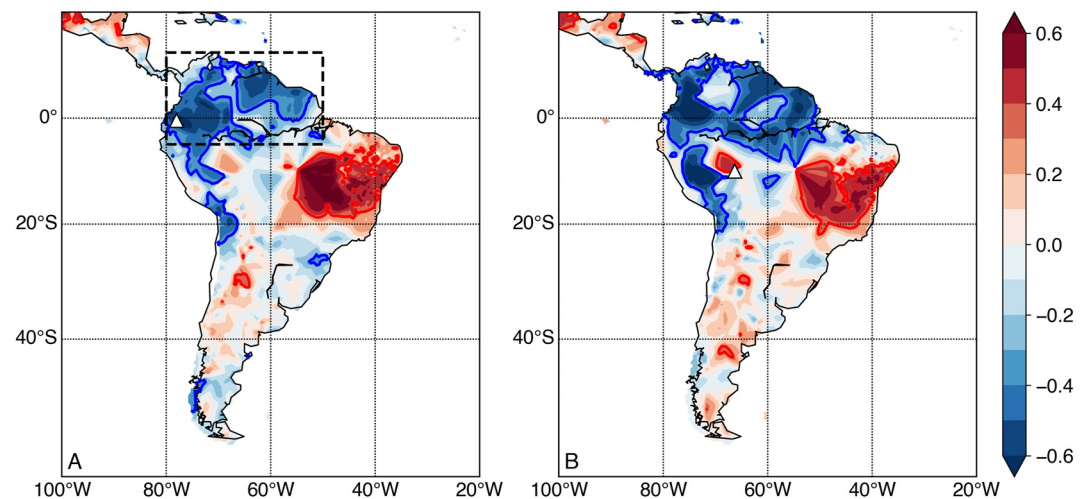
Figure 3. Correlations between $\delta^{18}O_{TR}$ and gridded precipitation. Maps show the relationship between the Ecuador (a) and Bolivia (b) $\delta^{18}O_{TR}$ records and precipitation from Climatic Research Unit for four months during the growing season (December–March, 1953–1989). White triangles show the location of the tree-ring sampling sites. The color bar indicates the strength of the correlation coefficients and blue and red contours show where correlations are significant ($p < 0.05$). The broken black line in (a) shows the area from which precipitation data were averaged in the time series shown in Figure 4.

Maps showing correlations between $\delta^{18}O_{TR}$ and gridded climate data can provide guidance about the causes of interannual variation and trends in $\delta^{18}O_{TR}$. Figure 3 shows correlations between Ecuador and Bolivia $\delta^{18}O_{TR}$ records and December–March CRU precipitation time series. These months coincide with the mature phase of the South American summer monsoon (SASM, Raia & Cavalcanti, 2008), and the growing season for *Cedrela* at each site. The emerging patterns for the two records are very similar, though the region of negative correlation extends further south for the Bolivia record. This corresponds to differences in pathways of moisture transport, with air parcels traveling to Ecuador over the more northern part of the basin (Figure S8 in Supporting Information S1). Both maps also show a clear dipole, with $\delta^{18}O_{TR}$ anticorrelated with precipitation over northern South America, but positively correlated with precipitation in the southeast of the Amazon basin. This anti-phasing between precipitation in the northeast Brazil and the rest of the basin has been observed before, and has been explained by strong moisture convergence and updraft over the basin driving higher rainfall, and corresponding subsidence of drier air in the surrounding regions (Bordi et al., 2015; Cruz et al., 2009). The dipole is modulated on orbital timescales (on the order of 10 kyr) by insolation affecting the intensity of the SASM: when summer insolation is high (low) in the southern hemisphere, a strong (weak) SASM strengthens (weakens) the Hadley and Walker circulations, increasing (reducing) subsidence and aridity in the region over northeast Brazil (Cruz et al., 2009).

Precipitation averaged over the north of the Amazon from December to March (region indicated in Figure 3a) correlates well with Ecuador $\delta^{18}O_{TR}$ ($r = -0.57$, $p < 0.001$, 1901–2012, $n = 112$), as does Amazon River discharge measured at Óbidos, which integrates precipitation over approximately 80% of the Amazon basin ($r = -0.63$, $p < 0.001$, 1903–2012, $n = 110$; Figure 4). Correlations with the Bolivia record are slightly stronger (Figure S9 in Supporting Information S1), this may be real or may be because the Bolivia record is slightly better constrained, as it has higher replication and lower inter-tree variability. A study analyzing climate signals in a $\delta^{18}O_{TR}$ chronology from the south of Ecuador found a better correlation with local CRU precipitation than with local station data, but the authors did not test for relationships with precipitation over a wider area (Volland et al., 2016) The authors hypothesize that moisture transported into the Andes from the Amazon is likely to influence $\delta^{18}O_{TR}$ in Ecuador, and the results presented here support this suggestion, with precipitation over the whole of northern South America affecting Ecuador $\delta^{18}O_{TR}$. No significant correlation between $\delta^{18}O_{TR}$ and local or regional temperature was found once variation in regional precipitation had been accounted for (Table S3 in Supporting Information S1). This in agreement with previous studies showing that temperature does not have an important influence on $\delta^{18}O_{TR}$ in the Amazon (Brienen et al., 2012; Volland et al., 2016) Overall, these results provide a strong indication that the Ecuador $\delta^{18}O_{TR}$ chronology is subject to the same controls as the Bolivia $\delta^{18}O_{TR}$ chronology, that is, successive precipitation events during moisture transport across the Amazon cause
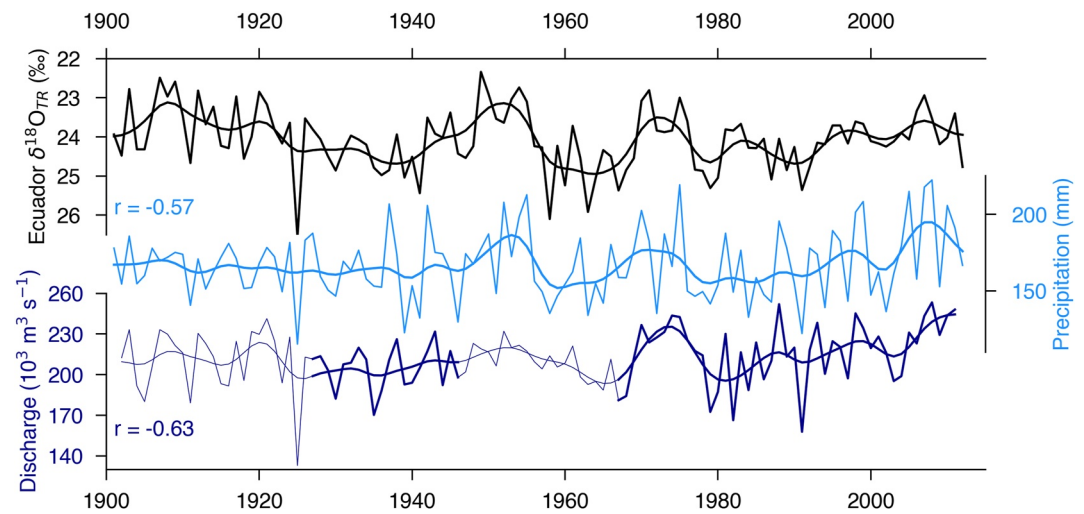
Figure 4. Effect of Amazon precipitation and runoff on $\delta^{18}O_{TR}$ from Ecuador. Interannual variation in the $\delta^{18}O_{TR}$ record from Ecuador (black line, scale reversed), precipitation from Climatic Research Unit averaged over the region indicated in Figure 3a (December–March, light blue line) and Amazon River discharge measured at Óbidos, which integrates precipitation over approximately 80% of the Amazon basin (June–August, dark blue line, line is thinner where data has been reconstructed from other river records). A low-pass Butterworth filter was applied to each series to visualize decadal variation. Values indicate the interannual Pearson correlation coefficients between $\delta^{18}O_{TR}$ and the other time series for the full period shown ($p < 0.001$). Note that the river data is offset because peak river flow lags peak precipitation by 4–6 months.

the progressive depletion of heavier water vapor isotopes (Dansgaard, 1964; Salati et al., 1979) and this signal is recorded in tree-ring cellulose.

To investigate larger-scale controls on Ecuador $\delta^{18}O_{TR}$ we correlated the annually-resolved record with SST data (Figure 5). The pattern of correlation is similar to that between the Quelccaya ice-core $\delta^{18}O$ record and SSTs (Figure 3 in Thompson et al., 2013), indicating that these Andean records have similar large-scale controls. The two main regions of influence are the equatorial Pacific, and the tropical North Atlantic. SST data extracted from these two regions (marked by broken lines in Figure 5a) were plotted as time series (Figures 5b and 5c). Previous work in the Amazon has highlighted the influence of Pacific SSTs on $\delta^{18}O_{TR}$ via the influence of the El Niño-Southern Oscillation (ENSO; Ballantyne et al., 2011; Brienen et al., 2012; Volland et al., 2016), and the effect on our $\delta^{18}O_{TR}$ record from Bolivia is particularly strong (Figure S10 in Supporting Information S1). However, this is the first time an important Atlantic influence has been shown, and thus is our focus here. Tropical North Atlantic SSTs correlate with Ecuador $\delta^{18}O_{TR}$ at interannual and decadal timescales (Figure 5b). We over-plotted the start points of 10-day back-trajectories from our sample site to provide some indication of the origin of water vapor relative to the regions of highest correlation (Figure S11 in Supporting Information S1). It is interesting to observe that most of these points fall in between the two regions of positive correlation in the Atlantic, suggesting that the effect of SSTs on $\delta^{18}O_{TR}$ is not direct (i.e., does not result from temperature-dependent fractionation during evaporation from the sea surface). Instead, it can be explained through a significant inverse relationship between tropical North Atlantic SSTs and precipitation upstream of our sample site, in the Guyanas and eastern Venezuela (December–March, Figure S12a in Supporting Information S1). Pacific SSTs affect precipitation in a similar but wider area over the same time period (Figure S12b in Supporting Information S1). An Atlantic control on Amazon hydrology has only been well understood in recent decades: warm (cold) tropical North Atlantic SSTs cause the northward (southward) displacement of the inter-tropical convergence zone (ITCZ), thus driving lower (higher) precipitation in the basin, predominantly during the dry season (Espinoza et al., 2011; Fernandes et al., 2011; Marengo et al., 2011; Yoon, 2016; Yoon & Zeng, 2010; Zeng et al., 2008). Our results show that tropical North Atlantic SSTs also significantly influence precipitation over the northern Amazon at the height of the wet season (December–March), which in turn affects the signal recorded in $\delta^{18}O_{TR}$. Differences in temperature trends between the Pacific and Atlantic have also been shown to have an important influence on Amazon hydrology. In recent decades, a combination of Atlantic warming and Pacific cooling has been associated with a strengthening of the equatorial Walker circulation and an increase in the frequency of extreme flood events in the Amazon (Barichivich et al., 2018).
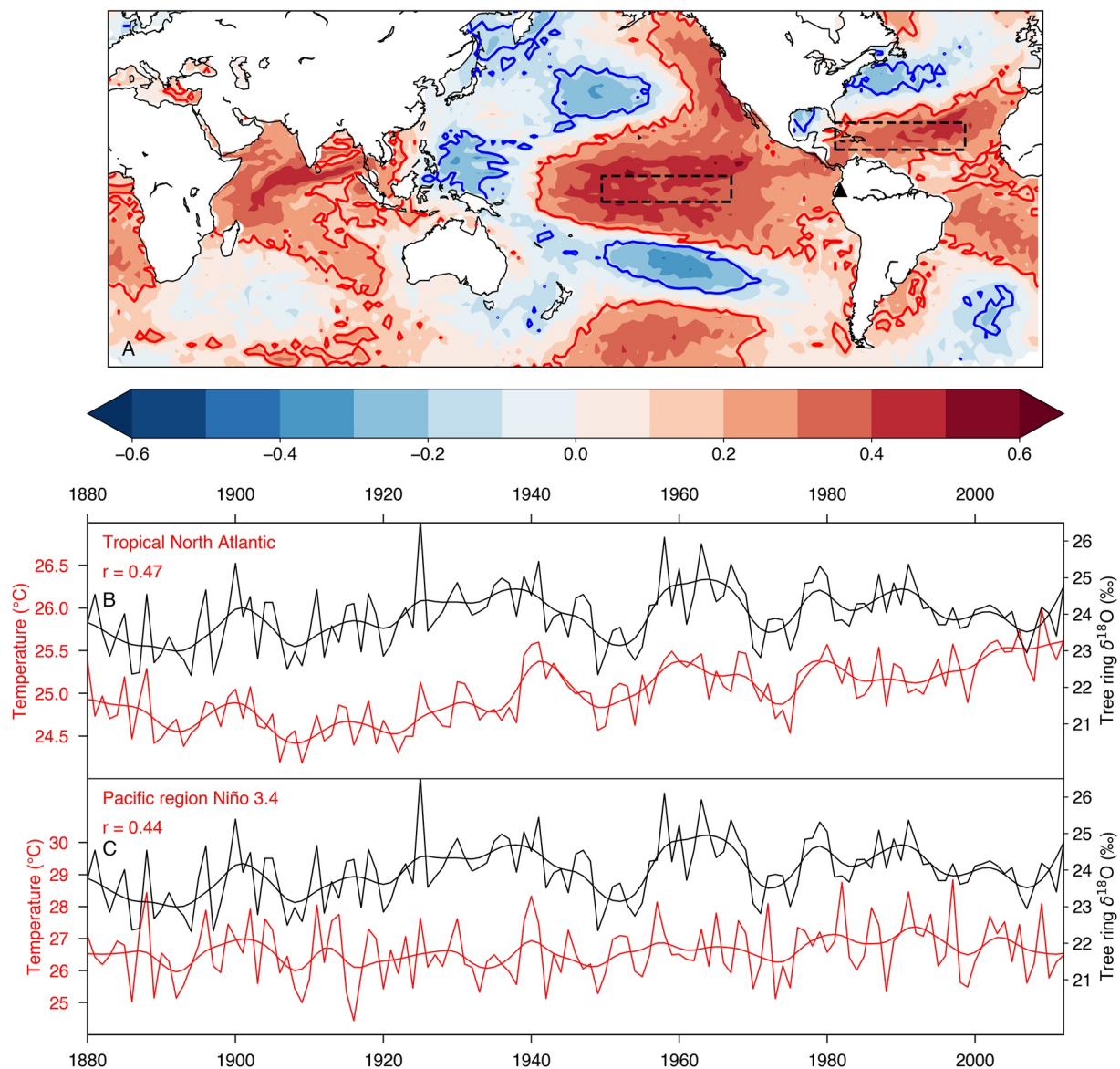
Figure 5. Correlation between $\delta^{18}O_{TR}$ from Ecuador and sea surface temperature (SST) data. (a) Map showing the relationship between the $\delta^{18}O_{TR}$ record from Ecuador and gridded SST data from NOAA for 4 months during the growing season (December–March, 1880–2012). The location of the $\delta^{18}O_{TR}$ sample site is indicated by a black triangle. The color bar indicates the strength of the correlation coefficients and blue and red contours show where correlations are significant ($p < 0.05$). Broken black lines indicate regions from which SST data were averaged in the time series shown in panels (b) and (c) (b) Interannual variation in SSTs from the tropical North Atlantic (red line) and the Ecuador $\delta^{18}O_{TR}$ record (black line). (c) As in (b), but for SSTs from the Niño 3.4 region of the Pacific. A low-pass Butterworth filter was applied to each series to visualize decadal variation. Values indicate the interannual Pearson correlation coefficients between $\delta^{18}O_{TR}$ and the other time series for the full period shown ($p < 0.001$).

3.3. Long-Term Trends in $\delta^{18}O_{TR}$

Both records show a significant positive trend in $\delta^{18}O_{TR}$ over their full length. The trend in the Ecuador record is 1.24‰ 100 year^{-1} ($p < 0.001$, 1799–2012) and in Bolivia 0.37‰ 100 year^{-1} ($p < 0.001$, 1860–2014). However, the trends are not constant through time. Both series show strong upward trends in $\delta^{18}O_{TR}$ in the period before 1900 (i.e., 2.11 and 2.43‰ 100 year^{-1} for 1860–1900, Ecuador and Bolivia respectively), but after 1900 the trends become gradually weaker, reaching a plateau at approximately 1950, and even becoming negative in the last 1–2 decades. In this section we focus on the long Ecuador record, which shows approximately a 3‰ increase from around 1800 to 1950. Similar (but weaker) positive trends over the past two centuries have been observed in other $\delta^{18}O$ proxy records, predominantly from the western part of the Amazon basin, including ice
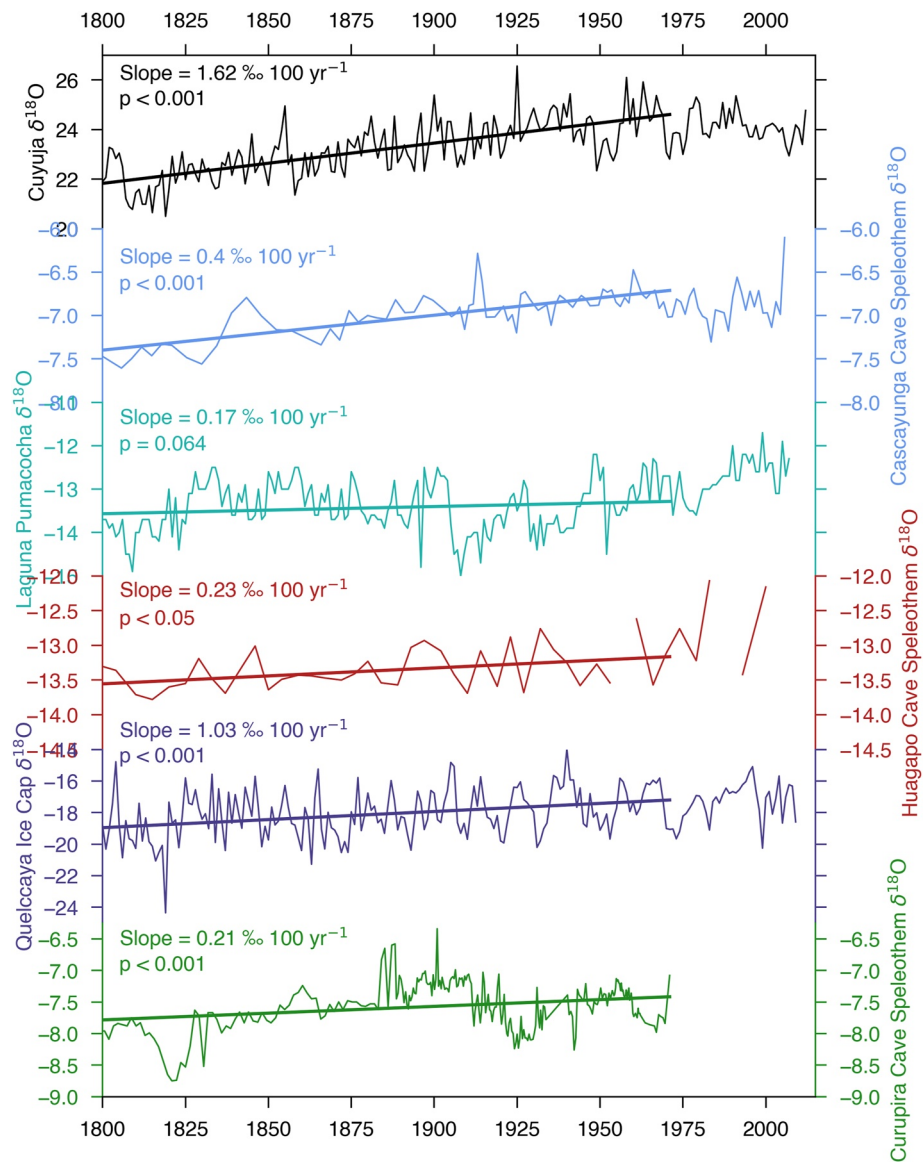
Figure 6. Long-term trends in different $\delta^{18}O$ proxy records from the Amazon. Interannual variation in $\delta^{18}O$ in tree rings from Ecuador (black line; this study), Cascayunga cave speleothem (light blue line; Reuter et al., 2009), lake sediment (cyan line; Bird et al., 2011), Huagapo cave speleothem (red line; Kanner et al., 2013), Quelccaya ice core (dark blue line; Thompson et al., 2013) and Curupira cave speleothem (green line; Novello et al., 2016). The locations of these records are shown in Figure 1. Significant trends for the common period of 1800–1971 are shown, and the slopes of the trend lines are indicated.

cores, lake sediments and speleothems (Figure 6). These trends range from 0.17 to 1.03‰ 100 year^{-1} for the common period of 1800–1971. The common long-term increase in different proxy records suggests that at least part of the increase in $\delta^{18}O_{TR}$ is due to an increase in $\delta^{18}O_P$, although the rate of $\delta^{18}O$ increase is the strongest in the tree-ring record. This might be related to the fact the site is the furthest north, or due to some influence of tree physiology, or because the trees only grow, and thus selectively record $\delta^{18}O$, for a few months during the Amazon wet season. Long-term increases in Amazon $\delta^{18}O$ records from lake sediment, ice cores and speleothems have previously been interpreted as showing a reduction in precipitation during the SASM (e.g., Bird et al., 2011; Kanner et al., 2013; Vuille et al., 2012). However, as this is the first study to evaluate long-term trends in Amazon $\delta^{18}O_{TR}$, we have compiled a list of hypotheses to explain the observed increase in $\delta^{18}O_{TR}$ over the past two centuries (Table 1). We discuss each hypothesis in turn and attempt to quantify how much (if any), of the long-term $\delta^{18}O_{TR}$ trend each factor is likely to explain.

Table 1
Summary of Hypotheses for the Long-Term Increase in $\delta^{18}O_{TR}$

Factor	Predicted contribution to the increase in $\delta^{18}O_{TR}$ (‰)
Ontogenetic effects	0
Tree-level response to increasing atmospheric CO_2	0.39
Changes in the leaf-to-air vapor pressure difference	0.61
Increase in seawater $\delta^{18}O$ at moisture origin	0
Effect of increasing sea surface temperatures on fractionation during evaporation from the ocean surface	0.086
Change in the lapse rate	0.13
Change in local amount effects	0
Direct effect of temperature on biosynthetic fractionation	0
Reduction in rainout fraction over the Amazon	1.78
Total	3.00

Note. The estimated contribution of each factor (deduced below) is shown.

3.3.1. Testing for an Ontogenetic Influence on $\delta^{18}O_{TR}$

When analyzing long isotope series, it is important to consider the possible influence of ontogeny. Our records are mostly constructed from large discs; thus, the early part of the record contains more juvenile rings than the later part, and therefore any age-related biases might result in erroneous trends in $\delta^{18}O_{TR}$. Work on juniper trees from Pakistan first revealed age biases in $\delta^{18}O_{TR}$, with series from juvenile trees showing negative trends in $\delta^{18}O_{TR}$ not evident in $\delta^{18}O_{TR}$ series from older trees over the same time period (Treydte et al., 2006). Since then, it has become apparent that the direction of ontogenetic biases can differ between different species and across climatic zones, with negative (Esper et al., 2010) and positive (Labuhn et al., 2014) age biases being reported, and other studies which find no significant ontogenetic influence on $\delta^{18}O_{TR}$ (Kilroy et al., 2016; Sano et al., 2013; Xu et al., 2016; Young et al., 2011). Given this variability, it is important to check whether there is any evidence for an effect of ontogeny on our *Cedrela* $\delta^{18}O_{TR}$ records from the Amazon.

To test for an ontogenetic influence on $\delta^{18}O_{TR}$ from Selva Negra, for each year from 2001 to 2010 we calculated the mean $\delta^{18}O_{TR}$ value for that year using only small trees (<20 cm diameter at breast height (DBH), 10 trees in total) and only large trees (>60 cm DBH, 9 trees in total). $\delta^{18}O_{TR}$ values in small and large trees were found to be highly correlated ($R^2 = 0.92$, Figure S13a in Supporting Information S1), and the slope of the regression is not significantly different from 1 (0.85 ± 0.21, 95% confidence interval). This is a strong indication that there is no effect of ontogeny on $\delta^{18}O_{TR}$ in *C. odorata*. It was not possible to use the same approach to test for ontogenetic effects in *C. montana* as we did not have sufficient data from small trees. Instead, we plotted the $\delta^{18}O_{TR}$ values from the seven old *C. montana* trees that included isotope measurements from young rings (<20 cm DBH) and older rings (>20 cm DBH), using different colors to differentiate between the two phases. $\delta^{18}O_{TR}$ values in young rings closely follow the values and trends in older rings and there are no trailing sections, which might be expected if there were strong trends during the early years of growth (Figure S13b in Supporting Information S1). Overall, we conclude that ontogeny does not have an important influence on $\delta^{18}O_{TR}$ in either of the records presented in this study and there was thus no need to apply de-trending procedures to remove biological age trends. This means that our records can be used to assess low frequency variation in climate. We next explore possible environmental drivers for the upward trend in $\delta^{18}O_{TR}$.

3.3.2. Tree-Level Response to Rising CO_2

The upward trend in $\delta^{18}O_{TR}$ could be related to the rise in atmospheric CO_2 since the Industrial Revolution, which may have affected trees' stomatal conductance and transpiration rates (e.g., Keenan et al., 2013; van der Sleen et al., 2015). Observations from Free Air CO_2 Enrichment (FACE) experiments show that trees dynamically reduce their stomatal conductance (g_s) in response to elevated CO_2 to optimize carbon gain (Ainsworth & Long, 2005). Studies have also highlighted increasing structural adaptations, with plants reducing the physical capacity of their leaves to conduct water as CO_2 rises, by changing stomatal density and/or size (de Boer et al., 2011; Lammertsma et al., 2011). Experiments show that plants have higher leaf cellulose $\delta^{18}O$ when g_s is

reduced (e.g., Barbour & Farquhar, 2000; Barbour et al., 2000), partly due to g_s affecting the transpiration rate. Transpiration is inversely related to the isotope enrichment of bulk leaf water ($\delta^{18}O_L$), as the flow of unenriched water from the stem opposes the back diffusion of enriched water from the site of evaporation into the rest of the leaf (i.e., the Péclet effect; Cernusak & Kahmen, 2013; Farquhar & Lloyd, 1993). Analyses on tree cores from FACE experiments in temperate sites have shown that elevated CO_2 (150–200 ppm above ambient) and the resulting reductions in g_s can cause small but significant increases in $\delta^{18}O_{TR}$, showing that $\delta^{18}O_L$ signals can be transferred to stem cellulose (Battipaglia et al., 2013). Thus, we may ask, can the $\delta^{18}O_{TR}$ increase of 3‰ be explained by this effect of? Increasing CO_2 has been estimated to reduce maximum g_s (g_{max}) by an average of 0.34% ppm^{-1} (Lammertsma et al., 2011), so an industrial atmospheric CO_2 increase of approximately 120 ppm, due to fossil fuel burning and cement production, might therefore be expected to have caused reductions in g_{max} on the order of 40%. Using the Péclet-modified Craig-Gordon (PMCG) model, as described by Farquhar and Lloyd (1993), Sternberg (2009) and others, we estimate that a 40% reduction in g_s would cause <0.4‰ increase in $\delta^{18}O_{TR}$ (Text S3 and Table S4 in Supporting Information S1). Therefore, while the increase in atmospheric CO_2 may contribute to the positive trend we observe, it is unlikely to be the primary driver.

3.3.3. Changes in Leaf-to-Air Vapor Pressure Difference

Humidity and (to a lesser extent) temperature (T) changes affect the degree of fractionation during evaporation from the leaf (e.g., Cernusak et al., 2016), and thus influence $\delta^{18}O_L$. For example, controlled greenhouse experiments on cotton plants showed that a 33% reduction in relative humidity (RH) increased $\delta^{18}O_L$ by 3–4‰ (Barbour & Farquhar, 2000). Kahmen et al. (2011) investigated the effect of leaf-to-air water vapor pressure difference (VPD, determined by RH and T), on $\delta^{18}O$ in different plant tissues of *Metrosideros polymorpha* along an altitudinal gradient in Hawaii. They used a mechanistic model of plant physiology to explore the effect of variation in VPD on cellulose $\delta^{18}O$. Although the $\delta^{18}O$ of xylem water decreased with elevation, they found that leaf and stem cellulose $\delta^{18}O$ increased, due to increasing VPD at higher altitudes. An increase in VPD might therefore contribute to the observed long-term increase in Ecuador $\delta^{18}O_{TR}$.

We consider local changes in T and RH to quantify the potential influence of VPD on $\delta^{18}O_{TR}$. Station data from the Andes show that local temperatures have increased by an average of 0.68°C since 1939 (Vuille et al., 2008). We can use this value, together with present-day measurements of T (10.5°C) and RH (90%) from the Papallacta meteorological station (2003–2012), to estimate the change in RH since 1939. Saturation vapor pressure (e_s) is calculated from T with the equation: $e_s = 0.6108e^{(17.27 \times T)/(T+237.3)}$ (e.g., Karamouz et al., 2012) and actual vapor pressure (e_a) with: $e_a = RH \times e_s$. Conservatively assuming that e_a has remained constant, we estimate that RH has decreased by 4% over the last eight decades. Using the PMCG model we calculated that a T rise of 0.68°C and a RH decrease of 4% would cause $\delta^{18}O_{TR}$ to increase by approximately 0.6‰ (Table S4 in Supporting Information S1). In combination with the response to increased CO_2 (Section 3.3.2), plant physiological responses might thus explain circa 1‰ of the 3‰ increase in $\delta^{18}O_{TR}$ over the past 200 years. This could explain why tree rings record a stronger increase in $\delta^{18}O$ than other proxy records from the Amazon (Figure 6). However, it is also necessary to acknowledge the limitations of our calculations. We used typical literature-derived parameter values, which are not specific for our species or site, and thus introduce a degree of uncertainty. Furthermore, work in the Australian tropics casts doubt on whether enrichment at the leaf level may be preserved in stem cellulose at all, due to plasticity in the extent of post-photosynthetic exchange reactions under varying levels of humidity (Cheesman & Cernusak, 2016; Voelker & Meinzer, 2017). Therefore, our estimated 1‰ contribution of leaf level enrichment to the increase in $\delta^{18}O_{TR}$ could rather be considered a maximum estimate of plant physiological influence.

3.3.4. Increase in Seawater $\delta^{18}O$ at Moisture Origin

The trend in $\delta^{18}O_{TR}$ could be driven by an increase in ocean surface $\delta^{18}O$ ($\delta^{18}O_{SW}$) in the region of evaporation. This could be due to a shift in the origin of source water, though previous work has shown that spatial variation in $\delta^{18}O_{SW}$ in the main source region for the Amazon is low (<1‰; Baker et al., 2016). Alternatively, there could be temporal variation in $\delta^{18}O_{SW}$. This can be tested over recent decades by looking at trends in surface seawater salinity, which is often (though not always) linearly related to $\delta^{18}O_{SW}$ (Craig & Gordon, 1965; LeGrande & Schmidt, 2006). Observations and model simulations of ocean salinity since 1950 have shown that enhanced evaporation from warming oceans has caused surface salinity to increase over most of the Atlantic (Durack et al., 2012; Durack & Wijffels, 2010). However, the main moisture source region for our site (inferred from the cluster of gray crosses in Figure S11 in Supporting Information S1) corresponds to a region where salinity has

seen a weak but significant decline since 1950 (Figure 5b in Durack & Wijffels, 2010). Thus, it seems unlikely that $\delta^{18}O_{SW}$ would have enriched over the same time-period. In addition, global seawater $\delta^{18}O$ has only changed by approximately 1‰ since the Last Glacial Maximum (Schrag et al., 2002), so changes larger than this in the last two centuries would also not be expected.

3.3.5. Effect of Increasing SSTs on Fractionation During Evaporation From the Ocean Surface

Temperature-dependent fractionation during evaporation from the surface of a body of water is well understood (e.g., Craig & Gordon, 1965; Majoube, 1971; Mook, 2000). The relationship between fractionation and temperature is inverse, as at higher temperatures there is a smaller difference between the amount of energy needed to evaporate light and heavy molecules of water and therefore fractionation is lower (Mook, 2000). The fractionation between liquid water and water vapor ($\varepsilon_{v/l}$, approximately equal to $\delta^{18}O_{liquid} - \delta^{18}O_{vapor}$) can be calculated using the equation from Majoube (1971) reformulated as in Mook (2000): $\varepsilon_{v/l} = -7356/T + 15.38$ where T is the temperature in kelvin. Using this we calculated that an SST increase of 1°C (e.g., 1900–2000, Figure 5b) would result in just a 0.086‰ increase in the isotopic composition of evaporated vapor. To achieve the 3‰ increase in $\delta^{18}O$ seen in the tree-ring record an improbable 35°C SST rise would be needed. From this we infer that temperature-driven reductions in fractionation during evaporation from the moisture source are not an important driver of the long-term trend in $\delta^{18}O_{TR}$.

3.3.6. Change in the Lapse Rate

In a previous study an increase in the lapse rate (the rate of temperature change with altitude in °C km^{-1}) was suggested to explain an increase in the offset between lowland and highland $\delta^{18}O$ records from the Amazon during the Younger Dryas (van Breukelen et al., 2008). Observation and model data from the Andes show rates of warming increase with altitude, and this trend is projected to continue over the next century (Bradley et al., 2006; Vuille et al., 2003, 2008). Since there is less isotope fractionation at higher temperatures (e.g., Mook, 2000) it is possible that faster warming at high altitudes since 1800 has steadily reduced the depletion of atmospheric water vapor during orographic precipitation, possibly explaining the increase in our highland $\delta^{18}O_{TR}$ record. The isotope lapse rate (the rate of change in $\delta^{18}O_P$ with altitude in ‰ km^{-1}) divided by the temperature lapse rate gives the expected isotope change per degree of warming (‰ °C^{-1}). This allows us to calculate the temperature change that would be required to explain the 3‰ increase in $\delta^{18}O_{TR}$. We used mean annual $\delta^{18}O_P$ and temperature data from a transect along the eastern Ecuadorian Andes, which passes close to our sample site, to calculate the isotope and temperature lapse rates (Garcia et al., 1998). Highland data come from Papallacta (3,150 m a.s.l.) and lowland data from Lago Agrio (297 m a.s.l.). Our calculated isotope lapse rate of −1.3‰ km^{-1} is approximately half the global average of −2.8‰ km^{-1} (Poage & Chamberlain, 2001). Using the regional (global) isotope lapse rate our calculations show that a 12.8°C (5.8°C) temperature rise would be needed at our sample site relative to the lowlands to explain the 3‰ rise in $\delta^{18}O_{TR}$. The Andes have seen a temperature rise of 0.68°C from 1939 to 2006 (Vuille et al., 2008) while CRU temperature data shows the Amazon region as a whole has warmed by 0.14°C over the same period. Thus, the increased warming in the highlands could only explain around 0.13‰ of the increase in $\delta^{18}O_{TR}$.

3.3.7. A Change in Local Amount Effects During Moisture Transport

The local "amount effect" refers to the inverse relationship between precipitation amount per unit time (e.g., mm month^{-1}) and the isotope composition of that precipitation (Dansgaard, 1964). Raindrops become further enriched as they fall through the air, due to re-evaporation and diffusive exchange processes between the rain droplets and the surrounding water vapor (Risi et al., 2008). However, these enrichment processes are less effective during heavy precipitation events as rain falls more quickly and RH is high, and as a result less of the heavy isotopes are removed during heavy rainfall events (i.e., the precipitation is isotopically lighter). We can conduct a thought experiment to imagine the influence of a change in local amount effects during rainfall events along the moisture transport trajectory over the basin on $\delta^{18}O_P$ (and thus $\delta^{18}O_{TR}$). In two scenarios the same volume of precipitation occurs along a trajectory, such that the fraction of water vapor remaining in the atmosphere at the end of the trajectory (i.e., our study site) is the same in each case. In the first scenario, all of the precipitation falls during a single heavy rainfall event, while in the second scenario there is continuous light precipitation along the full length of the trajectory. Although the total remaining water vapor is the same in each case, vapor will be isotopically heavier at the end of the trajectory in the first scenario than in the second scenario. Aerosols in smoke from fires in the Amazon have been shown to cause delays in the onset of precipitation and increase the frequency

of heavy rainfall events (Andreae et al., 2004). Therefore, an increase in biomass burning in the region may have caused changes in local amount effects (i.e., by shifting rainout patterns toward scenario 1). However, the effect of smoke on clouds in the Amazon is minimal during the wet season (Andreae et al., 2004), which is the period relevant for this study. Therefore, we do not expect our $\delta^{18}O_{TR}$ record to be strongly affected by changes in local amount effects.

3.3.8. Direct Effect of Temperature on Biosynthetic Fractionation

During photosynthesis, biosynthetic fractionation results in carbohydrates that are enriched in $\delta^{18}O$ by approximately 27‰ relative to source water (Sternberg, 2009; Sternberg et al., 1986). The degree of enrichment has been shown to vary with temperature, with little variation between 20°C and 30°C but a quasi-linear increase in fractionation as temperatures fall below 20°C, at a rate of approximately 0.3‰ per degree of cooling (Sternberg & Ellsworth, 2011). At Cuyuja, where mean annual temperature is 10.5°C, a local temperature decrease of around 10°C would have been needed to an explain a 3‰ increase in $\delta^{18}O_{TR}$. Temperatures in this region have increased rather than decreased (at least since 1939, Vuille et al., 2008). We also observe long-term $\delta^{18}O_{TR}$ increases in the Bolivia record, where mean annual temperature is 25°C–26°C, and therefore temperature effects on biosynthetic fractionation are expected to be minimal. We therefore conclude that this effect cannot explain the long-term trends in $\delta^{18}O_{TR}$ reported here.

3.3.9. A Reduction in Rainout Fraction Over the Amazon

The final environmental driver for increasing $\delta^{18}O_{TR}$ that we consider is a reduction in the proportion of incoming water vapor to the Amazon that falls as precipitation over the basin (i.e., rainout fraction), an idea that was first proposed by Brienen et al. (2012). We showed in Section 3.2 that $\delta^{18}O_{TR}$ from Ecuador and Bolivia record interannual and decadal variation in Amazon hydrology, modulated by Pacific and Atlantic SSTs. The long-term increase in $\delta^{18}O_{TR}$ and other $\delta^{18}O$ proxy records (Figure 6) could, therefore, reflect a reduction in precipitation during the wet season, provided the amount of incoming water vapor remained the same. Several studies have interpreted lake sediment, ice-core and speleothem $\delta^{18}O$ records from the Amazon in this way and suggest that the reduction in precipitation was driven by temperature increases over the North Atlantic forcing a northward shift in the ITCZ (Bird et al., 2011; Vuille et al., 2012). A second interpretation of the upward trend in $\delta^{18}O_{TR}$, not considered by these studies, is that it is caused by an increase in the volume of water vapor coming into the Amazon, which, if the amount of precipitation remained constant, would reduce the proportion of vapor that rains out. Both of these mechanisms would cause a reduction in the rainout fraction over the Amazon. Using the Rayleigh distillation equation: $\delta^{18}O_{VAP}(t) = \left(1,000 + \delta^{18}O_{VAP}(0)\right) \cdot f(t)^{(\alpha-1)} - 1,000$ we can calculate that the fraction (f) of vapor remaining in the atmosphere at time t (i.e., at our sample site) must have increased by approximately 25% to cause a 3‰ rise in vapor $\delta^{18}O$ ($\delta^{18}O_{VAP}$; assuming a temperature-dependent fractionation factor [α] of 1.0102 [calculated from a temperature of 15°C], and an initial water vapor $\delta^{18}O$ ($\delta^{18}O_{VAP}(0)$) of −11‰). Though this sounds large, Bordi et al. (2015) used ERA-Interim reanalysis data to show that total column water vapor has increased by around 13% over the Amazon since 1979, which is comparable with another analysis (using the same reanalysis data set) showing that wet season water vapor import to the Amazon has increased by approximately 15% over the same period, due to warming SSTs in the TNA (Gloor et al., 2015). Thus a 25% increase in incoming water vapor could feasibly explain the full 3‰ increase in $\delta^{18}O_{TR}$ since 1800. Alternatively, the increase could also be caused by a 25% reduction in wet season precipitation over the same timeframe, and there are insufficient instrumental data over the relevant period to confirm or refute this. Furthermore, if we deduct the 1.22‰ that can possibly already be explained by other hypotheses (Table 1) then only a 16% reduction in rainout fraction from either mechanism is required over the last two centuries.

Since both a reduction in precipitation and an increase in incoming water vapor have been associated with increasing tropical North Atlantic SSTs, we examined historical Atlantic SST data to look for support that the long-term increase in $\delta^{18}O_{TR}$ could be caused by a reduction in rainout fraction through either of these mechanisms. As instrumental data is not available back to 1800, we used a decadal North Atlantic SST reconstruction from Mann et al. (2009). It should be noted that this reconstructed SST data set is for the full North Atlantic, not just the tropical region. The reconstruction is based on 1,138 proxy datasets, including tree-ring, ice-core, speleothem, coral and marine sediment records. Our filtered Ecuador $\delta^{18}O_{TR}$ chronology shows a close resemblance to the reconstructed SST record up until approximately 1970, after which the records correspond less well ($r = 0.52$, $p < 0.001$, 1799–2006, Figure 7). Furthermore, both series show an upward trend over the past 200 years. Therefore, we suggest that warming SSTs since 1800 have driven a long-term reduction in rainout fraction over the
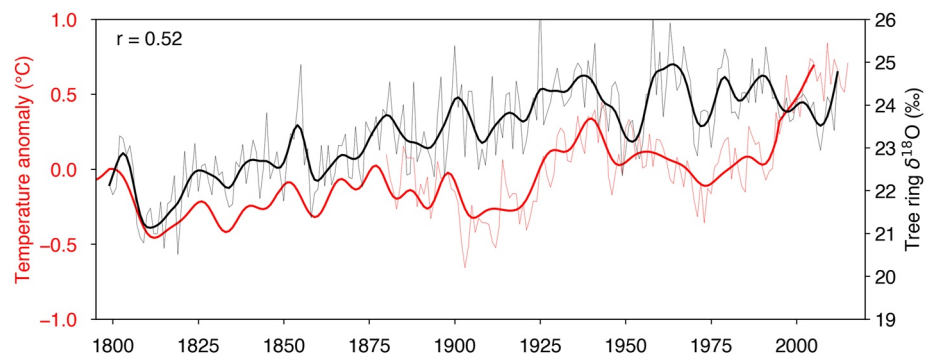
Figure 7. Relationship between $\delta^{18}O_{TR}$ from Ecuador and sea surface temperatures in the North Atlantic (NA SST). The thick red line shows reconstructed decadal NA SST data from Mann et al. (2009), who estimated SSTs using a large proxy data set. Observed annual mean NA SST anomalies from NOAA are also shown from 1880 for comparison against the reconstructed data (thin red line; averaged over 0–60°N, 75.5–7.5°W). In both cases anomalies are defined relative to a 1961–1990 reference period. Thick and thin black lines respectively indicate decadal and interannual variation in $\delta^{18}O_{TR}$ from Ecuador. A low-pass Butterworth filter was applied to the interannual $\delta^{18}O_{TR}$ record to visualize decadal variability. The Pearson correlation coefficient between the Mann NA SST reconstruction and decadal $\delta^{18}O_{TR}$ is 0.52 (1799–2006, $p < 0.001$).

Amazon, which has caused an increase in wet season $\delta^{18}O_P$ and this signal is recorded in tree rings in the west of the basin. The mechanism by which Atlantic SSTs affect the rainout fraction remains ambiguous. It could be by determining the position of the ITCZ and therefore affecting the amount of precipitation over the basin (see Section 3.2), or by controlling the amount of moisture supplied to the Amazon region and thus influencing proportional rainout. An isotope-enabled general circulation model (GCM) could possibly be used to resolve this current ambiguity.

3.4. The Recent Intensification of the Amazon Hydrological Cycle

The long-term increase in $\delta^{18}O_{TR}$ levels out in the middle of the 20th century, and reverses over the most recent period (Figure 2 and Figure S7 in Supporting Information S1). We explore whether this is consistent with the recent amplification of the Amazon hydrological cycle, characterized by increased precipitation seasonality in recent decades (e.g., Fu et al., 2013; Gloor et al., 2013). Both records show declines in $\delta^{18}O_{TR}$ over the past 1–2 decades, though this is particularly notable in the Bolivia record, with a decline in the maxima since the mid-1990s and the lowest value in the whole chronology observed in 2008. The 2008/2009 wet season coincided with one of the most severe flood events ever recorded in the Amazon, and the highest ever maximum water level at Óbidos (Marengo & Espinoza, 2016). The difference between the Ecuador and Bolivia records may be due to the fact that Ecuador $\delta^{18}O_{TR}$ is more influenced by precipitation in the northern part of the basin (Figure 3) and precipitation over this region (light blue line in Figure 4) hasn't increased as much as it has over the whole basin (dark blue line in Figure 4; see also Gloor et al., 2013). Gloor et al. (2015) suggest the amplification of Amazon hydrology may be due to increased warming in the Atlantic, coupled with a switch to the cold phase of the Pacific Decadal Oscillation (PDO) in the 1990s. Model experiments have revealed an important teleconnection between the Atlantic and Pacific oceans, with increased Atlantic warming driving an acceleration of Pacific trade winds, subduction of heat in the Pacific and colder Pacific SSTs (England et al., 2014; McGregor et al., 2014). The Atlantic Multidecadal Oscillation (AMO) also changed from a cold to a warm phase in the 1990s, which, superimposed on anthropogenic warming has resulted in an "unprecedented" cross-basin difference in SSTs, a strengthening of the Walker circulation (Barichivich et al., 2018) and increased precipitation over the Amazon basin (Kucharski et al., 2016; McGregor et al., 2014). We argue that the recent flattening, or even decline in $\delta^{18}O_{TR}$ is a result of the increase in wet season precipitation associated with a strengthened Amazon hydrological cycle, which has reversed the long-term upward trend in $\delta^{18}O_{TR}$ over the past two centuries.

4. Summary

This paper aimed to identify what $\delta^{18}O_{TR}$ records from the Amazon can teach us about changes in Amazon hydrology on inter-annual and multi-decadal to centennial timescales. We present the two longest $\delta^{18}O_{TR}$ records from the Amazon basin to date, which extend substantially beyond the limit of regional hydrological data. The chronologies from Bolivia and Ecuador show coherent isotope signatures, indicating they are governed by climate controls operating at the basin scale. Our analyses show that $\delta^{18}O_{TR}$ from Bolivia and Ecuador provide a record of interannual variation in basin-wide precipitation and the factors that control it. Furthermore, we find that both chronologies show a long-term increase in $\delta^{18}O_{TR}$, which is the clearest evidence yet of a long-term increase in wet season $\delta^{18}O_P$ in the western Amazon over the past 200 years. The increase in $\delta^{18}O_{TR}$ is related to a gradual rise in SSTs in the North Atlantic over the same period. The mechanism behind the Atlantic influence could either be through a reduction in precipitation over the basin caused by a northward shift of the ITCZ, or by rising SSTs causing an increase in water vapor imported to the basin. Both mechanisms would result in a reduction in the rainout fraction over the Amazon basin, but they cannot be distinguished without additional evidence, possibly from an isotope-enabled GCM. The upward trend has reversed in recent decades, consistent with an intensification of the Amazon hydrological cycle since the 1990s.

Data Availability Statement

The $\delta^{18}O_{TR}$ data presented in the study are available via https://doi.org/10.5281/zenodo.7105508. Climate data used in the study were obtained from https://climexp.knmi.nl/start.cgi.

References

Ainsworth, E. A., & Long, S. P. (2005). What have we learned from 15 years of free-air CO$_2$ enrichment (FACE)? A meta-analytic review of the responses of photosynthesis, canopy properties and plant production to rising CO$_2$. *New Phytologist*, *165*(2), 351–372. https://doi.org/10.1111/j.1469-8137.2004.01224.x

Andreae, M. O., Rosenfeld, D., Artaxo, P., Costa, A. A., Frank, G. P., Longo, K. M., & Silva-Dias, M. A. F. (2004). Smoking rain clouds over the Amazon. *Science*, *303*(5662), 1337–1342. https://doi.org/10.1126/science.1092779

Andreu-Hayles, L., Ummenhofer, C. C., Barriendos, M., Schleser, G. H., Helle, G., Leuenberger, M., et al. (2016). 400 Years of summer hydroclimate from stable isotopes in Iberian trees. *Climate Dynamics*, *49*(1–2), 1–19. https://doi.org/10.1007/s00382-016-3332-z

Antico, A., & Torres, M. E. (2015). Evidence of a decadal solar signal in the Amazon River: 1903 to 2013. *Geophysical Research Letters*, *42*(24), 10782–10787. https://doi.org/10.1002/2015gl066089

Baker, J. C. A., Garcia-Carreras, L., Buermann, W., Castilho De Souza, D., Marsham, J. H., Kubota, P. Y., et al. (2021). Robust Amazon precipitation projections in climate models that capture realistic land–atmosphere interactions. *Environmental Research Letters*, *16*(7), 074002. https://doi.org/10.1088/1748-9326/abfb2e

Baker, J. C. A., Gloor, M., Boom, A., Neill, D. A., Cintra, B. B. L., Clerici, S. J., & Brienen, R. J. W. (2018). Questioning the influence of sunspots on amazon hydrology: Even a broken clock tells the right time twice a day. *Geophysical Research Letters*, *45*(3), 1419–1422. https://doi.org/10.1002/2017gl076889

Baker, J. C. A., Gloor, M., Spracklen, D. V., Arnold, S. R., Tindall, J. C., Clerici, S. J., et al. (2016). What drives interannual variation in tree ring oxygen isotopes in the Amazon? *Geophysical Research Letters*, *43*(22), 11831–11840. https://doi.org/10.1002/2016gl071507

Baker, J. C. A., Hunt, S. F. P., Clerici, S. J., Newton, R. J., Bottrell, S. H., Leng, M. J., et al. (2015). Oxygen isotopes in tree rings show good coherence between species and sites in Bolivia. *Global and Planetary Change*, *133*, 298–308. https://doi.org/10.1016/j.gloplacha.2015.09.008

Baker, J. C. A., Santos, G. M., Gloor, M., & Brienen, R. J. W. (2017). Does Cedrela always form annual rings? Testing ring periodicity across South America using radiocarbon dating. *Trees*, *31*(6), 1–11. https://doi.org/10.1007/s00468-017-1604-9

Ballantyne, A. P., Baker, P. A., Chambers, J. Q., Villalba, R., & Argollo, J. (2011). Regional differences in South American monsoon precipitation inferred from the growth and isotopic composition of tropical trees. *Earth Interactions*, *15*(5), 1–35. https://doi.org/10.1175/2010ei277.1

Barbour, M. M., & Farquhar, G. D. (2000). Relative humidity- and ABA-induced variation in carbon and oxygen isotope ratios of cotton leaves. *Plant, Cell and Environment*, *23*(5), 473–485. https://doi.org/10.1046/j.1365-3040.2000.00575.x

Barbour, M. M., Fischer, R. A., Sayre, K. D., & Farquhar, G. D. (2000). Oxygen isotope ratio of leaf and grain material correlates with stomatal conductance and grain yield in irrigated wheat. *Functional Plant Biology*, *27*(7), 625–637. https://doi.org/10.1071/pp99041

Barbour, M. M., Roden, J. S., Farquhar, G. D., & Ehleringer, J. R. (2004). Expressing leaf water and cellulose oxygen isotope ratios as enrichment above source water reveals evidence of a Péclet effect. *Oecologia*, *138*(3), 426–435. https://doi.org/10.1007/s00442-003-1449-3

Barichivich, J., Gloor, E., Peylin, P., Brienen, R. J. W., Schöngart, J., Espinoza, J. C., & Pattnayak, K. C. (2018). Recent intensification of Amazon flooding extremes driven by strengthened Walker circulation. *Science Advances*, *4*(9), eaat8785. https://doi.org/10.1126/sciadv.aat8785

Battipaglia, G., Saurer, M., Cherubini, P., Calfapietra, C., McCarthy, H. R., Norby, R. J., & Francesca Cotrufo, M. (2013). Elevated CO$_2$ increases tree-level intrinsic water use efficiency: Insights from carbon and oxygen isotope analyses in tree rings across three forest FACE sites. *New Phytologist*, *197*(2), 544–554. https://doi.org/10.1111/nph.12044

Bird, B. W., Abbott, M. B., Vuille, M., Rodbell, D. T., Stansell, N. D., & Rosenmeier, M. F. (2011). A 2, 300-year-long annually resolved record of the South American summer monsoon from the Peruvian Andes. *Proceedings of the National Academy of Sciences*, *108*(21), 8583–8588. https://doi.org/10.1073/pnas.1003719108

Boettger, T., Haupt, M., Knöller, K., Weise, S. M., Waterhouse, J. S., Rinne, K. T., et al. (2007). Wood cellulose preparation methods and mass spectrometric analyses of $\delta^{13}C$, $\delta^{18}O$, and nonexchangeable δ^2H values in cellulose, sugar, and starch: An interlaboratory comparison. *Analytical Chemistry*, *79*(12), 4603–4612. https://doi.org/10.1021/ac0700023

Boisier, J. P., Ciais, P., Ducharne, A., & Guimberteau, M. (2015). Projected strengthening of Amazonian dry season by constrained climate model simulations. *Nature Climate Change*, *5*(7), 656–660. https://doi.org/10.1038/nclimate2658

Bordi, I., De Bonis, R., Fraedrich, K., & Sutera, A. (2015). Interannual variability patterns of the world's total column water content: Amazon River basin. *Theoretical and Applied Climatology*, *122*(3–4), 441–455. https://doi.org/10.1007/s00704-014-1304-y

Bradley, R. S. (2011). High-resolution Paleoclimatology. In M. K. Hughes, T. W. Swetnam, & H. F. Diaz (Eds.), *Dendroclimatology: Progress and prospects*. Springer Netherlands.

Bradley, R. S., Vuille, M., Diaz, H. F., & Vergara, W. (2006). Threats to water supplies in the tropical Andes. *Science*, *312*(5781), 1755–1756. https://doi.org/10.1126/science.1128087

Bräuning, A., Volland-Voigt, F., Burchardt, I., Ganzhi, O., Nauss, T., & Peters, T. (2009). Climatic control of radial growth of *Cedrela montana* in a humid mountain rainforest in southern Ecuador. *Erdkunde*, *63*(4), 337–345. https://doi.org/10.3112/erdkunde.2009.04.04

Bräuning, A., Von Schnakenburg, P., Volland-Voigt, F., & Peters, T. (2008). Seasonal growth dynamics and its climate forcing in a tropical mountain rain forest in southern Ecuador. In *TRACE Tree Rings in Archaeology Climatology Ecology* (Vol. *6*, 27–30).

Brienen, R. J. W., Helle, G., Pons, T. L., Guyot, J. L., & Gloor, M. (2012). Oxygen isotopes in tree rings are a good proxy for Amazon precipitation and El Niño-Southern Oscillation variability. *Proceedings of the National Academy of Sciences*, *109*(42), 16957–16962. https://doi.org/10.1073/pnas.1205977109

Brienen, R. J. W., Schöngart, J., & Zuidema, P. A. (2016). Tree rings in the tropics: Insights into the ecology and climate Sensitivity of tropical trees. In G. Goldstein & L. S. Santiago (Eds.), *Tropical tree physiology: Adaptations and responses in a changing environment*. Springer International Publishing.

Brienen, R. J. W., & Zuidema, P. A. (2005). Relating tree growth to rainfall in Bolivian rain forests: A test for six species using tree ring analysis. *Oecologia*, *146*, 1–12. https://doi.org/10.1007/s00442-005-0160-y

Cernusak, L. A., Barbour, M. M., Arndt, S. K., Cheesman, A. W., English, N. B., Feild, T. S., et al. (2016). Stable isotopes in leaf water of terrestrial plants. *Plant, Cell and Environment*, *39*(5), 1087–1102. https://doi.org/10.1111/pce.12703

Cernusak, L. A., & Kahmen, A. (2013). The multifaceted relationship between leaf water O enrichment and transpiration rate. *Plant, Cell and Environment*, *36*(7), 1239–1241. https://doi.org/10.1111/pce.12081

Cheesman, A., & Cernusak, L. (2016). Infidelity in the outback: Climate signal recorded in $\Delta^{18}O$ of leaf but not branch cellulose of eucalypts across an Australian aridity gradient. *Tree Physiology*, *37*(5), 554–564. https://doi.org/10.1093/treephys/tpw121

Cintra, B. B. L., Gloor, M., Boom, A., Schöngart, J., Baker, J. C. A., Cruz, F. W., et al. (2021). Tree-ring oxygen isotopes record a decrease in Amazon dry season rainfall over the past 40 years. *Climate Dynamics*, *59*(5–6), 1401–1414. https://doi.org/10.1007/s00382-021-06046-7

Cox, P. M., Betts, R. A., Collins, M., Harris, P. P., Huntingford, C., & Jones, C. D. (2004). Amazonian forest dieback under climate-carbon cycle projections for the 21st century. *Theoretical and Applied Climatology*, *78*(1–3), 137–156. https://doi.org/10.1007/s00704-004-0049-4

Craig, H., & Gordon, L. I. (1965). Deuterium and oxygen 18 variations in the ocean and the marine atmosphere. In E. Tongiogi (Ed.), *Stable isotopes in oceanographic studies and paleotemperatures*. Consiglio nazionale delle richerche, Laboratorio de geologia nucleare.

Cruz, F. W., Vuille, M., Burns, S. J., Wang, X., Cheng, H., Werner, M., et al. (2009). Orbitally driven east–west antiphasing of South American precipitation. *Nature Geoscience*, *2*(3), 210–214. https://doi.org/10.1038/ngeo444

Dansgaard, W. (1964). Stable isotopes in precipitation. *Tellus*, *16*(4), 436–468. https://doi.org/10.1111/j.2153-3490.1964.tb00181.x

de Boer, H. J., Lammertsma, E. I., Wagner-Cremer, F., Dilcher, D. L., Wassen, M. J., & Dekker, S. C. (2011). Climate forcing due to optimization of maximal leaf conductance in subtropical vegetation under rising CO_2. *Proceedings of the National Academy of Sciences*, *108*(10), 4041–4046. https://doi.org/10.1073/pnas.1100555108

Durack, P. J., & Wijffels, S. E. (2010). Fifty-year trends in global ocean salinities and their relationship to broad-scale warming. *Journal of Climate*, *23*(16), 4342–4362. https://doi.org/10.1175/2010jcli3377.1

Durack, P. J., Wijffels, S. E., & Matear, R. J. (2012). Ocean salinities reveal strong global water cycle intensification during 1950 to 2000. *Science*, *336*(6080), 455–458. https://doi.org/10.1126/science.1212222

England, M. H., McGregor, S., Spence, P., Meehl, G. A., Timmermann, A., Cai, W., et al. (2014). Recent intensification of wind-driven circulation in the Pacific and the ongoing warming hiatus. *Nature Climate Change*, *4*(3), 222–227. https://doi.org/10.1038/nclimate2106

Esper, J., Frank, D. C., Battipaglia, G., Büntgen, U., Holert, C., Treydte, K., et al. (2010). Low-frequency noise in δ13C and δ18O tree ring data: A case study of *Pinus uncinata* in the Spanish Pyrenees. *Global Biogeochemical Cycles*, *24*(4), 1–11. https://doi.org/10.1029/2010gb003772

Espinoza, J. C., Marengo, J. A., Ronchail, J., Carpio, J. M., Flores, L. N., & Guyot, J. L. (2014). The extreme 2014 flood in south-western Amazon basin: The role of tropical-subtropical South Atlantic SST gradient. *Environmental Research Letters*, *9*(12), 1–9. https://doi.org/10.1088/1748-9326/9/12/124007

Espinoza, J. C., Ronchail, J., Guyot, J. L., Junquas, C., Vauchel, P., Lavado, W., et al. (2011). Climate variability and extreme drought in the upper Solimões River (western Amazon Basin): Understanding the exceptional 2010 drought. *Geophysical Research Letters*, *38*(13), 1–6. https://doi.org/10.1029/2011gl047862

Farquhar, G., & Lloyd, J. (1993). Carbon and oxygen isotope effects in the exchange of carbon dioxide between terrestrial plants and the atmosphere. *Stable Isotopes and Plant Carbon-Water Relations*, *40*, 47–70. https://doi.org/10.1016/b978-0-08-091801-3.50011-8

Fernandes, K., Baethgen, W., Bernardes, S., DeFries, R., DeWitt, D. G., Goddard, L., et al. (2011). North Tropical Atlantic influence on western Amazon fire season variability. *Geophysical Research Letters*, *38*(12), 1–5. https://doi.org/10.1029/2011gl047392

Fu, R., Yin, L., Li, W., Arias, P. A., Dickinson, R. E., Huang, L., et al. (2013). Increased dry-season length over southern Amazonia in recent decades and its implication for future climate projection. *Proceedings of the National Academy of Sciences*, *110*(45), 18110–18115. https://doi.org/10.1073/pnas.1302584110

Garcia, M., Villalba, F., Araguas-Araguas, L., & Rozanski, K. (1998). The role of atmospheric circulation patterns in controlling the regional distribution of stable isotope contents in precipitation: Preliminary results from two transects in the Ecuadorian Andes. In *Isotope techniques in the study of environmental change* (pp. 127–140). International Atomic Energy Agency (IAEA).

Gärtner, H., & Nievergelt, D. (2010). The core-microtome: A new tool for surface preparation on cores and time series analysis of varying cell parameters. *Dendrochronologia*, *28*(2), 85–92. https://doi.org/10.1016/j.dendro.2009.09.002

Gatti, L., Gloor, M., Miller, J., Doughty, C., Malhi, Y., Domingues, L., et al. (2014). Drought sensitivity of Amazonian carbon balance revealed by atmospheric measurements. *Nature*, *506*(7486), 76–80. https://doi.org/10.1038/nature12957

Gloor, M., Barichivich, J., Ziv, G., Brienen, R. J. W., Schöngart, J., Peylin, P., et al. (2015). Recent Amazon climate as background for possible ongoing and future changes of Amazon humid forests. *Global Biogeochemical Cycles*, *29*(9), 1384–1399. https://doi.org/10.1002/2014gb005080

Gloor, M., Brienen, R. J. W., Galbraith, D., Feldpausch, T. R., Schöngart, J., Guyot, J. L., et al. (2013). Intensification of the Amazon hydrological cycle over the last two decades. *Geophysical Research Letters*, *40*(9), 1729–1733. https://doi.org/10.1002/grl.50377

Harris, I., Jones, P. D., Osborn, T. J., & Lister, D. H. (2014). Updated high-resolution grids of monthly climatic observations–the CRU TS3.10 Dataset. *International Journal of Climatology*, *34*(3), 623–642. https://doi.org/10.1002/joc.3711

HidroWeb. (2018). *HidroWeb, Brazilian Water Resources Database. Water Resources National Agency, Brazil*. Agência Nacional de Águas.

Huang, B., Banzon, V. F., Freeman, E., Lawrimore, J., Liu, W., Peterson, T. C., et al. (2015). Extended reconstructed sea surface temperature version 4 (ERSST. v4). Part I: Upgrades and intercomparisons. *Journal of Climate*, *28*(3), 911–930. https://doi.org/10.1175/jcli-d-14-00006.1

Huang, B., Thorne, P. W., Smith, T. M., Liu, W., Lawrimore, J., Banzon, V. F., et al. (2016). Further exploring and quantifying uncertainties for extended reconstructed sea surface temperature (ERSST) version 4 (v4). *Journal of Climate*, *29*(9), 3119–3142. https://doi.org/10.1175/jcli-d-15-0430.1

Huntingford, C., Fisher, R. A., Mercado, L., Booth, B. B. B., Sitch, S., Harris, P. P., et al. (2008). Towards quantifying uncertainty in predictions of Amazon 'dieback'. *Philosophical Transactions of the Royal Society B: Biological Sciences*, *363*(1498), 1857–1864. https://doi.org/10.1098/rstb.2007.0028

Insel, N., Poulsen, C. J., Sturm, C., & Ehlers, T. A. (2013). Climate controls on Andean precipitation δ^{18}O interannual variability. *Journal of Geophysical Research: Atmospheres*, *118*(17), 9721–9742. https://doi.org/10.1002/jgrd.50619

Kagawa, A., Sano, M., Nakatsuka, T., Ikeda, T., & Kubo, S. (2015). An optimized method for stable isotope analysis of tree rings by extracting cellulose directly from cross-sectional laths. *Chemical Geology*, *393*, 16–25. https://doi.org/10.1016/j.chemgeo.2014.11.019

Kahmen, A., Sachse, D., Arndt, S. K., Tu, K. P., Farrington, H., Vitousek, P. M., & Dawson, T. E. (2011). Cellulose δ^{18}O is an index of leaf-to-air vapor pressure difference (VPD) in tropical plants. *Proceedings of the National Academy of Sciences*, *108*(5), 1981–1986. https://doi.org/10.1073/pnas.1018906108

Kanner, L. C., Burns, S. J., Cheng, H., Edwards, R. L., & Vuille, M. (2013). High-resolution variability of the South American summer monsoon over the last seven millennia: Insights from a speleothem record from the central Peruvian Andes. *Quaternary Science Reviews*, *75*, 1–10. https://doi.org/10.1016/j.quascirev.2013.05.008

Karamouz, M., Nazif, S., & Falahi, M. (2012). *Hydrology and hydroclimatology: Principles and applications*. CRC Press.

Keenan, T. F., Hollinger, D. Y., Bohrer, G., Dragoni, D., Munger, J. W., Schmid, H. P., & Richardson, A. D. (2013). Increase in forest water-use efficiency as atmospheric carbon dioxide concentrations rise. *Nature*, *499*(7458), 324–327. https://doi.org/10.1038/nature12291

Kilroy, E., McCarroll, D., Young, G. H., Loader, N. J., & Bale, R. J. (2016). Absence of juvenile effects confirmed in stable carbon and oxygen isotopes of European larch trees. *Acta Silvae et Ligni*, *111*, 27–33. https://doi.org/10.20315/asetl.111.3

Kucharski, F., Ikram, F., Molteni, F., Farneti, R., Kang, I.-S., No, H.-H., et al. (2016). Atlantic forcing of Pacific decadal variability. *Climate Dynamics*, *46*(7–8), 2337–2351. https://doi.org/10.1007/s00382-015-2705-z

Labuhn, I., Daux, V., Pierre, M., Stievenard, M., Girardclos, O., Feron, A., et al. (2014). Tree age, site and climate controls on tree ring cellulose delta O-18: A case study on oak trees from south-western France. *Dendrochronologia*, *32*(1), 78–89. https://doi.org/10.1016/j.dendro.2013.11.001

Lammertsma, E. I., de Boer, H. J., Dekker, S. C., Dilcher, D. L., Lotter, A. F., & Wagner-Cremer, F. (2011). Global CO_2 rise leads to reduced maximum stomatal conductance in Florida vegetation. *Proceedings of the National Academy of Sciences*, *108*(10), 4035–4040. https://doi.org/10.1073/pnas.1100371108

LeGrande, A. N., & Schmidt, G. A. (2006). Global gridded data set of the oxygen isotopic composition in seawater. *Geophysical Research Letters*, *33*(12), 1–5. https://doi.org/10.1029/2006gl026011

Lewis, S. L., Brando, P. M., Phillips, O. L., Van Der Heijden, G. M., & Nepstad, D. (2011). The 2010 amazon drought. *Science*, *331*(6017), 554. https://doi.org/10.1126/science.1200807

Li, Z.-H., Labbé, N., Driese, S. G., & Grissino-Mayer, H. D. (2011). Micro-scale analysis of tree-ring δ^{18}O and δ^{13}C on α-cellulose spline reveals high-resolution intra-annual climate variability and tropical cyclone activity. *Chemical Geology*, *284*(1–2), 138–147. https://doi.org/10.1016/j.chemgeo.2011.02.015

Loader, N. J., Robertson, I., Lucke, A., & Helle, G. (2002). Preparation of holocellulose from standard increment cores for stable carbon isotope analysis. *Swansea Geographer*, *37*, 1–9.

Majoube, M. (1971). Fractionnement en oxygène-18 et en deutérium entre l'eau et sa vapeur. *Journal de Chimie Physique et de Physico-Chimie Biologique*, *58*(18), 1423–1435. https://doi.org/10.1051/jcp/1971681423

Malhi, Y., Aragão, L. E., Galbraith, D., Huntingford, C., Fisher, R., Zelazowski, P., et al. (2009). Exploring the likelihood and mechanism of a climate-change-induced dieback of the Amazon rainforest. *Proceedings of the National Academy of Sciences*, *106*(49), 20610–20615. https://doi.org/10.1073/pnas.0804619106

Mann, M. E., Zhang, Z., Rutherford, S., Bradley, R. S., Hughes, M. K., Shindell, D., et al. (2009). Global signatures and dynamical origins of the little ice age and medieval climate anomaly. *Science*, *326*(5957), 1256–1260. https://doi.org/10.1126/science.1177303

Marengo, J. A., & Espinoza, J. C. (2016). Extreme seasonal droughts and floods in Amazonia: Causes, trends and impacts. *International Journal of Climatology*, *36*(3), 1033–1050. https://doi.org/10.1002/joc.4420

Marengo, J. A., Tomasella, J., Alves, L. M., Soares, W. R., & Rodriguez, D. A. (2011). The drought of 2010 in the context of historical droughts in the Amazon region. *Geophysical Research Letters*, *38*(12), 1–5. https://doi.org/10.1029/2011gl047436

Mccarroll, D., & Loader, N. J. (2004). Stable isotopes in tree rings. *Quaternary Science Reviews*, *23*(7–8), 771–801. https://doi.org/10.1016/j.quascirev.2003.06.017

McGregor, S., Timmermann, A., Stuecker, M. F., England, M. H., Merrifield, M., Jin, F.-F., & Chikamoto, Y. (2014). Recent Walker circulation strengthening and Pacific cooling amplified by Atlantic warming. *Nature Climate Change*, *4*(10), 888–892. https://doi.org/10.1038/nclimate2330

Mook, W. G. (2000). *Environmental Isotopes in the Hydrological Cycle: Volume I Introduction (Theory, Methods, Review)*. International Atomic Energy Agency and United Nations Educational, Scientific and Cultural Organization.

Moquet, J., Cruz, F., Novello, V., Stríkis, N., Deininger, M., Karmann, I., et al. (2016). Calibration of speleothem δ^{18}O records against hydroclimate instrumental records in Central Brazil. *Global and Planetary Change*, *139*, 151–164. https://doi.org/10.1016/j.gloplacha.2016.02.001

Nobre, C. A., Obregón, G. O., Marengo, J. A., Fu, R., & Poveda, G. (2009). Characteristics of Amazonian climate: Main features. In *Amazonia and global change*. American Geophysical Union.

Novello, V. F., Vuille, M., Cruz, F. W., Stríkis, N. M., De Paula, M. S., Edwards, R. L., et al. (2016). Centennial-scale solar forcing of the South American Monsoon System recorded in stalagmites. *Scientific Reports*, *6*, 1–8. https://doi.org/10.1038/srep24762

Peterson, T. C., & Vose, R. S. (1997). An overview of the Global Historical Climatology Network temperature database. *Bulletin of the American Meteorological Society*, *78*(12), 2837–2849. https://doi.org/10.1175/1520-0477(1997)078<2837:aootgh>2.0.co;2

Phillips, O. L., Aragão, L. E., Lewis, S. L., Fisher, J. B., Lloyd, J., López-González, G., et al. (2009). Drought sensitivity of the Amazon rainforest. *Science*, *323*(5919), 1344–1347. https://doi.org/10.1126/science.1164033

Pierrehumbert, R. T. (1999). Huascaran δ^{18}O as an indicator of tropical climate during the last glacial maximum. *Geophysical Research Letters*, *26*(9), 1345–1348. https://doi.org/10.1029/1999gl900183

Poage, M. A., & Chamberlain, C. P. (2001). Empirical relationships between elevation and the stable isotope composition of precipitation and surface waters: Considerations for studies of paleoelevation change. *American Journal of Science*, *301*(1), 1–15. https://doi.org/10.2475/ajs.301.1.1

Raia, A., & Cavalcanti, I. F. A. (2008). The life cycle of the South American monsoon System. *Journal of Climate*, *21*(23), 6227–6246. https://doi.org/10.1175/2008jcli2249.1

Reuter, J., Stott, L., Khider, D., Sinha, A., Cheng, H., & Edwards, R. L. (2009). A new perspective on the hydroclimate variability in northern South America during the Little Ice Age. *Geophysical Research Letters*, *36*(21), 1–5. https://doi.org/10.1029/2009gl041051

Risi, C., Bony, S., & Vimeux, F. (2008). Influence of convective processes on the isotopic composition ($\delta^{18}O$ and δD) of precipitation and water vapor in the tropics: 2. Physical interpretation of the amount effect. *Journal of Geophysical Research*, *113*(D19), 1–12. https://doi.org/10.1029/2008jd009943

Salati, E., Dall'olio, A., Matsui, E., & Gat, J. R. (1979). Recycling of water in the Amazon basin: An isotopic study. *Water Resources Research*, *15*(5), 1250–1258. https://doi.org/10.1029/wr015i005p01250

Sano, M., Tshering, P., Komori, J., Fujita, K., Xu, C., & Nakatsuka, T. (2013). May–September precipitation in the Bhutan Himalaya since 1743 as reconstructed from tree ring cellulose $\delta^{18}O$. *Journal of Geophysical Research: Atmospheres*, *118*(15), 8399–8410. https://doi.org/10.1002/jgrd.50664

Schrag, D. P., Adkins, J. F., McIntyre, K., Alexander, J. L., Hodell, D. A., Charles, C. D., & McManus, J. F. (2002). The oxygen isotopic composition of seawater during the Last Glacial Maximum. *Quaternary Science Reviews*, *21*(1), 331–342. https://doi.org/10.1016/s0277-3791(01)00110-x

Sternberg, L., & Ellsworth, P. F. V. (2011). Divergent biochemical fractionation, not convergent temperature, explains cellulose oxygen isotope enrichment across latitudes. *PLoS One*, *6*(11), e28040. https://doi.org/10.1371/journal.pone.0028040

Sternberg, L. D. S. L. (2009). Oxygen stable isotope ratios of tree-ring cellulose: The next phase of understanding. *New Phytologist*, *181*(3), 553–562. https://doi.org/10.1111/j.1469-8137.2008.02661.x

Sternberg, L. D. S. L., Deniro, M. J., & Savidge, R. A. (1986). Oxygen isotope exchange between metabolites and water during biochemical reactions leading to cellulose synthesis. *Plant Physiology*, *82*(2), 423–427. https://doi.org/10.1104/pp.82.2.423

Stokes, M., & Smiley, T. (1968). *An introduction to tree-ring dating*. University of Arizona Press.

Thompson, L. G., Mosley-Thompson, E., Davis, M. E., Zagorodnov, V. S., Howat, I. M., Mikhalenko, V. N., & Lin, P. N. (2013). Annually resolved ice core records of tropical climate variability over the past ∼1800 years. *Science*, *340*(6135), 945–950. https://doi.org/10.1126/science.1234210

Treydte, K. S., Schleser, G. H., Helle, G., Frank, D. C., Winiger, M., Haug, G. H., & Esper, J. (2006). The twentieth century was the wettest period in northern Pakistan over the past millennium. *Nature*, *440*(7088), 1179–1182. https://doi.org/10.1038/nature04743

van Breukelen, M. R., Vonhof, H. B., Hellstrom, J. C., Wester, W. C. G., & Kroon, D. (2008). Fossil dripwater in stalagmites reveals Holocene temperature and rainfall variation in Amazonia. *Earth and Planetary Science Letters*, *275*(1–2), 54–60. https://doi.org/10.1016/j.epsl.2008.07.060

Van Der Sleen, P., Groenendijk, P., Vlam, M., Anten, N. P., Boom, A., Bongers, F., et al. (2015). No growth stimulation of tropical trees by 150 years of CO_2 fertilization but water-use efficiency increased. *Nature Geoscience*, *8*(1), 24–28. https://doi.org/10.1038/ngeo2313

Van Der Sleen, P., Zuidema, P. A., & Pons, T. L. (2017). Stable isotopes in tropical tree rings: Theory, methods and applications. *Functional Ecology*, *31*(9), 1674–1689. https://doi.org/10.1111/1365-2435.12889

Villacís, M., Vimeux, F., & Taupin, J. D. (2008). Analysis of the climate controls on the isotopic composition of precipitation ($\delta^{18}O$) at Nuevo Rocafuerte, 74.5 W, 0.9 S, 250 m, Ecuador. *Comptes Rendus Geoscience*, *340*, 1–9. https://doi.org/10.1016/j.crte.2007.11.003

Vimeux, F., Gallaire, R., Bony, S., Hoffmann, G., & Chiang, J. C. (2005). What are the climate controls on δD in precipitation in the Zongo valley (Bolivia)? Implications for the Illimani ice core interpretation. *Earth and Planetary Science Letters*, *240*(2), 205–220. https://doi.org/10.1016/j.epsl.2005.09.031

Voelker, S. L., & Meinzer, F. C. (2017). Where and when does stem cellulose $\delta^{18}O$ reflect a leaf water enrichment signal? *Tree Physiology*, *00*(5), 1–3. https://doi.org/10.1093/treephys/tpx029

Volland, F., Pucha, D., & Braeuning, A. (2016). Hydro-climatic variability in southern Ecuador reflected by tree-ring oxygen isotopes. *Erdkunde*, *70*(1), 69–82. https://doi.org/10.3112/erdkunde.2016.01.05

Vuille, M., Bradley, R. S., Werner, M., Healy, R., & Keimig, F. (2003). Modeling $\delta^{18}O$ in precipitation over the tropical Americas: 1. Interannual variability and climatic controls. *Journal of Geophysical Research*, *108*(D6), 1–24. https://doi.org/10.1029/2001jd002038

Vuille, M., Burns, S., Taylor, B., Cruz, F., Bird, B., Abbott, M., et al. (2012). A review of the South American monsoon history as recorded in stable isotopic proxies over the past two millennia. *Climate of the Past*, *8*(4), 1309–1321. https://doi.org/10.5194/cp-8-1309-2012

Vuille, M., Francou, B., Wagnon, P., Juen, I., Kaser, G., Mark, B. G., & Bradley, R. S. (2008). Climate change and tropical Andean glaciers: Past, present and future. *Earth-Science Reviews*, *89*(3–4), 79–96. https://doi.org/10.1016/j.earscirev.2008.04.002

Wang, X., Edwards, R. L., Auler, A. S., Cheng, H., Kong, X., Wang, Y., et al. (2017). Hydroclimate changes across the Amazon lowlands over the past 45,000 years. *Nature*, *541*(7636), 204–207. https://doi.org/10.1038/nature20787

Ward, B. M., Wong, C. I., Novello, V. F., Mcgee, D., Santos, R. V., Silva, L. C. R., et al. (2019). Reconstruction of Holocene coupling between the South American Monsoon System and local moisture variability from speleothem $\delta^{18}O$ and $^{87}Sr/^{86}Sr$ records. *Quaternary Science Reviews*, *210*, 51–63. https://doi.org/10.1016/j.quascirev.2019.02.019

Wieloch, T., Helle, G., Heinrich, I., Voigt, M., & Schyma, P. (2011). A novel device for batch-wise isolation of α-cellulose from small-amount wholewood samples. *Dendrochronologia*, *29*(2), 115–117. https://doi.org/10.1016/j.dendro.2010.08.008

Wigley, T. M., Briffa, K. R., & Jones, P. D. (1984). On the average value of correlated time series, with applications in dendroclimatology and hydrometeorology. *Journal of Climate and Applied Meteorology*, *23*(2), 201–213. https://doi.org/10.1175/1520-0450(1984)023<0201:otavoc>2.0.co;2

Wong, M. L., Wang, X., Latrubesse, E. M., He, S., & Bayer, M. (2021). Variations in the South Atlantic convergence zone over the mid-to-late holocene inferred from speleothem $\delta^{18}O$ in central Brazil. *Quaternary Science Reviews*, *270*, 107178. https://doi.org/10.1016/j.quascirev.2021.107178

Xu, C., Sano, M., & Nakatsuka, T. (2011). Tree ring cellulose $\delta^{18}O$ of *Fokienia hodginsii* in northern Laos: A promising proxy to reconstruct ENSO? *Journal of Geophysical Research*, *116*(D24), 1–12. https://doi.org/10.1029/2011jd016694

Xu, C. X., Ge, J. Y., Nakatsuka, T., Yi, L., Zheng, H. Z., & Sano, M. (2016). Potential utility of tree ring delta O-18 series for reconstructing precipitation records from the lower reaches of the Yangtze River, southeast China. *Journal of Geophysical Research: Atmospheres*, *121*(8), 3954–3968. https://doi.org/10.1002/2015jd023610

Yoon, J. H. (2016). Multi-model analysis of the Atlantic influence on Southern Amazon rainfall. *Atmospheric Science Letters*, *17*(2), 122–127. https://doi.org/10.1002/asl.600

Yoon, J.-H., & Zeng, N. (2010). An Atlantic influence on Amazon rainfall. *Climate Dynamics*, *34*(2–3), 249–264. https://doi.org/10.1007/s00382-009-0551-6

Young, G. H. F., Demmler, J. C., Gunnarson, B. E., Kirchhefer, A. J., Loader, N. J., & McCarroll, D. (2011). Age trends in tree ring growth and isotopic archives: A case study of *Pinus sylvestris* L. from northwestern Norway. *Global Biogeochemical Cycles*, *25*(2), 1–6. https://doi.org/10.1029/2010gb003913

Zemp, D. C., Schleussner, C.-F., Barbosa, H. M. J., Hirota, M., Montade, V., Sampaio, G., et al. (2017). Self-amplified Amazon forest loss due to vegetation-atmosphere feedbacks. *Nature Communications*, *8*, 1–10. https://doi.org/10.1038/ncomms14681

Zeng, N., Yoon, J.-H., Marengo, J. A., Subramaniam, A., Nobre, C. A., Mariotti, A., & Neelin, J. D. (2008). Causes and impacts of the 2005 Amazon drought. *Environmental Research Letters*, *3*(1), 1–9. https://doi.org/10.1088/1748-9326/3/1/014002